JCI The Journal of Clinical Investigation

A fibroblast-dependent TGFβ1/sFRP2 noncanonical Wnt signaling axis promotes epithelial metaplasia in idiopathic pulmonary fibrosis

Max L. Cohen, … , Harold A. Chapman, Claude Jourdan Le Saux

J Clin Invest. 2024. https://doi.org/10.1172/JCI174598.

Research In-Press Preview Pulmonology

Graphical abstract

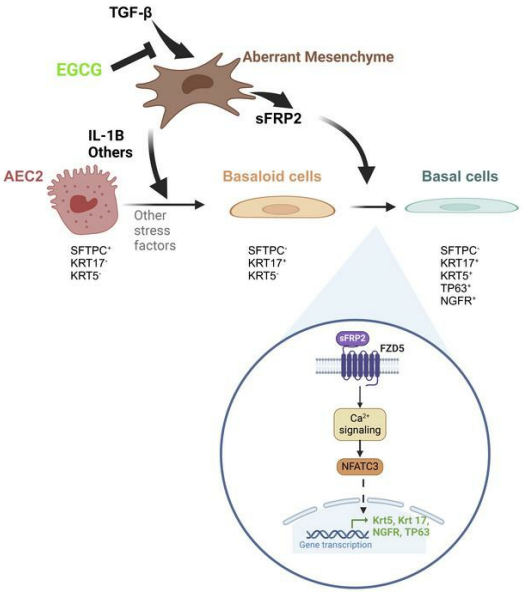

Title: A fibroblast-dependent TGFβ1/sFRP2 noncanonical Wnt signaling axis promotes epithelial metaplasia in idiopathic pulmonary fibrosis

Max L. Cohen[1*], Alexis N. Brumwell[1*], Tsung Che Ho[1], Kiana Garakani, Genevieve Montas[1], Darren Leong[1], Vivianne Ding[2], Jeffrey A. Golden[1], Binh N. Trinh[2], David Jablons[2], Michael A. Matthay[1], Kirk D. Jones[3], Paul J. Wolters[1], Ying Wei[1], Harold A. Chapman[1**], Claude Jourdan Le Saux[1**]

[1]Department of Medicine, Division of Pulmonary, Critical Care, Allergy, and Sleep Medicine; [2]Department of Surgery, Division of Cardiothoracic Surgery; [3]Department of Pathology; University of California San Francisco, San Francisco, California

*Co-first authors; **Co-senior authors.

Address correspondence to:

Hal Chapman, M.D.

University of California, San Francisco

513 Parnassus Ave, HSE Building, Room 201

San Francisco, CA 94143

Email: hal.chapman@ucsf.edu

Conflict of Interest Statement: MAM receives research funds from Roche-Genentech and Quantum Health; PJW owns equity shares in Illumina and BMS ; HAC is a co-founder with equity in Pliant Therapeutics and receives research funds from Pliant. JAG receives research funds to support corporate-sponsored clinical trials unrelated to this manusccipt from Roche, Daewoong, Pliant, United Therapeutics, Cumberland,Genentech, Bristol-Myers Squibb, and Glaxo Smith Kline. Other authors have no potential conflicts to declare.

Abstract
Reciprocal interactions between alveolar fibroblasts and epithelial cells are crucial for lung homeostasis, injury repair, and fibrogenesis, but underlying mechanisms remain unclear. To investigate, we administered the fibroblast-selective TGFβ1 signaling inhibitor, epigallocatechin gallate (EGCG), to Interstitial Lung Disease (ILD) patients undergoing diagnostic lung biopsy and conducted single-cell RNA sequencing on spare tissue. Biopsies from untreated patients showed higher fibroblast TGFβ1 signaling compared to non-disease donor or end-stage ILD tissues. *In vivo*, EGCG downregulated TGFβ1 signaling and several pro-inflammatory and stress pathways in biopsy samples. Notably, EGCG reduced fibroblast secreted frizzle-like receptor protein 2 (sFRP2), an unrecognized TGFβ1 fibroblast target gene induced near type II alveolar epithelial cells (AEC2s) in situ. Using AEC2-fibroblast coculture organoids and precision cut lung slices (PCLS) from non-diseased donors, we found TGFβ1 signaling promotes a spread AEC2 KRT17+ basaloid state, whereupon sFRP2 then activates a mature Krt5+ basal cell program. Wnt-receptor Frizzled 5 (Fzd5) expression and downstream calcineurin signaling were required for sFRP2-induced nuclear NFATc3 accumulation and KRT5 expression. These findings highlight stage-specific TGFβ1 signaling in ILD, the therapeutic potential of EGCG in reducing IPF-related transcriptional changes, and identify TGFβ1-non-canonical Wnt pathway crosstalk via sFRP2 as a mechanism for dysfunctional epithelial signaling in Idiopathic Pulmonary Fibrosis/ILD.

Main Text

Introduction

Fibrotic Interstitial Lung Diseases (ILDs) such as IPF cause respiratory failure through progressive replacement of lung parenchyma with nonfunctional fibrotic tissue. IPF is widely thought to be caused by epithelial dysfunction leading to fibroblast activation, extracellular matrix production, and further epithelial dysfunction, causing the *usual interstitial pneumonia* (UIP) pattern of tissue fibrosis (1-3). Histologically, the UIP pattern is characterized by heterogeneous parenchymal fibrosis, formation of subepithelial fibroblast foci, and alveolar epithelia loss and metaplasia, especially the formation of characteristic honeycomb cysts lined by “bronchiolized” epithelium (4-6), but the molecular & cellular basis of this pathological pattern is unclear. Recent single-cell RNA sequencing studies of IPF lung tissue confirmed loss of type 1 and 2 alveolar epithelial cells (AEC1 and AEC2, respectively) and identified the development of basaloid epithelium (7, 8). AEC2s normally have the dual function of producing pulmonary surfactant and differentiating into AEC1s, which line alveoli (9). However, in IPF, AEC2s can differentiate into cytokeratin 5 $(KRT5)^{+}$ basal cells (BC), normally found lining airways (10). This AEC2-to-BC metaplastic differentiation is regulated by fibroblast signaling, and promoted by the pleotropic growth factor TGFβ1, itself a key mediator of tissue remodeling in IPF (10). How these cellular epithelial abnormalities contribute to IPF histopathology and disease progression is not yet fully understood.

We have previously determined that trihydroxyphenolic compounds, such as epigallocatechin gallate (EGCG), cause fibroblast-specific TGFβ1 receptor kinase and lysyl oxidase like 2 (LOXL2) inhibition, thereby reducing fibroblast activation and collagen cross-linking in fibrotic mice lungs and in cultured human precision cut lung slices (PCLS) derived from IPF patients (11, 12). When taken for two weeks, EGCG reduced protein markers of pro-fibrotic signaling in

spare diagnostic surgical biopsy tissue from patients with ILD (13). However there was only limited transcriptional information. Here, we report the result of single-cell RNA sequencing of lung tissue from additional ILD patients who took EGCG for two weeks prior to diagnostic surgical biopsy, including comparison to normal donor and end-stage ILD explant lung tissues. The findings provide new insights into the scope of TGFβ1-dependent pro-fibrotic mediators increased in IPF and confirm their strong inhibition by EGCG. In the course of this work secreted frizzed related protein 2 (sFRP2) was identified as a TGFβ1-upregulated gene in fibroblasts *in vivo* that directly drives AEC2s toward basal cell metaplasia ex vivo, implicating sFRP2 as a strong mediator of pathological fibroblast-AEC2 interaction.

Results

Fibroblasts from ILD Biopsy samples have higher TGFβ1 signaling than IPF explants.

Eight patients with undiagnosed interstitial lung disease donated spare diagnostic biopsy tissue, half after taking EGCG (Figure 1A). Patients had mild disease based on most recent pulmonary function testing (Supplemental Table 1). We combined our single-cell RNA sequencing (scRNA-seq) files obtained from non-diseased donor lungs ("donor") samples, untreated biopsy samples ("untreated biopsy"), tissue from ILD patients undergoing lung transplantation for end-stage disease ("IPF explant"), and published samples from GSE135893 and GSE132771 (Figure 1B). The integrated transcriptomes of all samples contained various cell types which were identified by classical cell markers (Supplemental Figure 1). Subsequently, we focused our analyses on the transcriptome of the fibroblasts and epithelial cells (Figures 1 and 2). The sources and cell numbers for the fibroblasts and epithelial cell transcriptomes analyzed in this manuscript are provided in Supplemental Table 2.

We first assessed whether fibroblast transcriptomes evolved with ILD disease progression. Previously established gene markers for annotation of fibroblast subpopulations are detailed in Supplemental Figure 2A. Compared to donor samples, untreated biopsy samples show reduced alveolar fibroblasts and expansion of previously-defined pathological fibroblast subtypes (Collagen Triple Helix Repeat Containing 1^+ ($CTHRC1^+$), inflammatory, and $HAS1^+$/BMP $antagonist^+$) (Figure 1C) (8, 10, 14-17). Differential gene expression analysis of untreated ILD biopsy vs control (non-diseased) donor and untreated ILD biopsy vs IPF explant fibroblasts demonstrate transcriptional upregulation of numerous individual genes involved in the TGFβ-pathway (Figure 1D-F, Supplemental Figure 2B-D, Supplemental Table 3A). Single-cell pathway analysis identified higher TGFβ1 pathway activity in fibroblasts from untreated biopsies than from donor or ILD explants (1G). Upstream Ingenuity Pathway Analysis (IPA) confirmed up-regulation of TGFβ1 signaling in fibroblasts from untreated biopsy samples compared to donor samples, with TGFβ1 itself having the highest Z-score (13.5) of all upstream pathways (Figure 1H, Supplemental Table 3B). Notably, several inflammatory and stress pathways also had positive Z-scores above 5: TNFA, IFNG, IL6, STAT3, AGT, TEAD1, IL1B, P53, p38 MAPK, and MYC. Signaling associated with these pathways was increased in explant fibroblasts relative to donors, but was markedly higher in untreated biopsy than in explants (Figure 1H). Western blot analysis of lung tissue lysates from independent donor, untreated biopsy, and IPF explant samples demonstrates higher phosphor-SMAD3 (pSMAD3) expression in untreated ILD biopsies than in IPF explant samples (Supplemental Figure 2B-C), consistent with the transcriptomic changes. Pan-phosphotyrosine levels were not reduced in control biopsies (Supplemental Figure 2D), indicating that artifact or non-specific phosphatase activity is unlikely to explain altered pSmad3 levels. These data indicate that fibroblasts from ILD patients with mild disease undergoing diagnostic biopsy have higher TGFβ1 and pro-inflammatory pathway signaling than either donor tissue or end-stage explant ILD tissue. We next

determined to what degree treatment of IPF patients with EGCG for two weeks would inhibit TGFβ1 signaling.

TGFβ signaling in ILD fibroblasts is inhibited by EGCG. Transcriptomes from biopsy fibroblasts isolated from patients who took EGCG ("EGCG biopsies") daily for two weeks were compared to that of biopsies from patients who were untreated ("untreated biopsies"). Proximal (adventitial) fibroblasts, lipofibroblasts, and smooth muscle cell/myofibroblast transcriptomes were removed from the original dataset (Figure 1) to focus on fibroblasts residing near alveoli and/or appearing within the pathology, termed alveolar and pathologic (Figure 2A, Supplemental Figure 3A). Alveolar and pathologic fibroblast subtypes, including CTHRC1^{+}, inflammatory, and HAS1^{+}/BMP antagonist^{+}, were sub-setted and re-clustered. Notably, the alveolar fibroblast cluster in the patient-derived samples was comprised of cells with canonical alveolar fibroblast markers (e.g. INMT) but also subpopulations with inflammatory gene expression, e.g. CCL2 and CXCL12 (Supplemental Figure 2A), not usually seen in normal alveolar fibroblasts. Dimensional reduction and annotation of subtypes (Figure 2A, Supplemental Figure 3A) show trends toward altered fibroblast composition due to EGCG treatment, including fewer CTHRC1^{+} and more alveolar fibroblast subtypes (Figure 2A). Comparison of gene expression in fibroblasts in EGCG biopsy vs untreated biopsy samples demonstrates marked downregulation of individual TGFβ1 pathway genes, including types 1 and 6 fibrillar collagens, CTHRC1, and serpine-1 (PAI1), as well as other targets including sFRP2 (Figure 2B-D, Supplemental Table 3C). Upstream IPA confirmed down-regulation of TGFβ1 signaling due to EGCG treatment as well as down-regulation of multiple inflammatory (IL5, TNFA, IFNG, IL4, IL1B, IL6) and stress signaling pathways (TP53, p38 MAPK, XBP1, MYC) in fibroblasts (Figure 2C, Supplemental Table 3D), all of which were upregulated in untreated biopsy fibroblasts compared with donor controls (Figure 1D). Gene expression changes could not be explained by variation among

individual samples (Figure 2D). There was substantial overlap in the list of top 100 genes upregulated in untreated biopsy vs donor fibroblasts and the top 100 downregulated genes in EGCG biopsy vs untreated biopsy fibroblasts (Suplemental Figure 3B, Supplemental Table 3E), highlighting the central role of TGFβ1 signaling in fibrotic fibroblasts.

EGCG exposure reduced fibrosis-associated changes in epithelial cells. Following dimensional reduction and annotation using known markers of cell type (7, 8, 10, 16), the transcriptomes of epithelial cells were compared across sample type, donor, untreated biopsy, and EGCG biopsy (Figure 3A, Supplemental Figure 3C). A marked loss of AEC2s was already observed in untreated biopsy samples as previously reported in IPF explant lungs (7, 8), (Figure 3B; note that AEC2s are shown as percentage of nonciliated epithelium). Moreover, an upstream IPA on differentially-expressed genes in AEC2s from untreated biopsies compared to non-diseased donors had positive Z-scores for numerous inflammatory and stress pathways, e.g. IL6, TNFα, NFKB, JNK, TP53, DDX5, and p38 MAPK, as well as for TGFβ1. Even though the 2-week EGCG exposure did not reverse the loss of AEC2 seen in untreated biopsy, a near complete pattern reversal was measured on the mentioned differentially-expressed genes in AEC2s (Figure 3C, Supplemental Table 3F-G). The NicheNet receptor-ligand signaling prediction algorithm was used to infer altered signaling from fibroblast ligands to AEC2 receptors due to EGCG. Notably, signaling from numerous AEC2-supporting niche factors, such as multiple FGFs, WNT5A, BMP5, and HGF, was increased in the EGCG treated group (Figure 3D). Conversely, fibrosis-associated signaling pathways, such as collagens, CTGF, IL6, SERPINE1/PAI1, COMP, APOE, and TGFβ1, were all predicted to be decreased in EGCG-treated samples (Figure 3E). EGCG requires LOXL2 for its activation as a TGFβ1 kinase inhibitor. LOXL2 is not expressed in epithelial cells including AEC2s and hence EGCG has no

discernible direct effect on AEC2s (11). These findings suggest that inhibition of fibroblast TGFβ1 signaling by EGCG reduces fibroblast-mediated changes in alveolar epithelial cells.

Secreted Frizzled Related Protein 2 is a fibroblast-specific TGFβ1 gene target in IPF. Analysis of the fibroblast genes downregulated by inhibition of TGFβ1 signaling identified sFRP2 as one of the most downregulated genes, with a $\log_2$ fold change of -2.1 (Figure 2D, Figure 4A, Table Supplemental 3C). We confirmed that sFRP2 is a TGFβ1 target gene, based on strong and specific upregulation of *sFRP2* mRNA by TGFβ1 in primary human lung fibroblasts that was suppressed when a TGFβ1 inhibitor was added to the culture (Figure 4B). Moreover, among the five known human sFRPs, only sFRP2 is strongly upregulated by TGFβ1 (Supplemental Fig 4A) and inspection of several online sc-RNA sequencing files reveal that sFRP2 expression is specific to fibroblasts in ILD (7, 8, 17-19), and Rosas and Kropski online sc-RNA sequence files in IPF ATLAS.COM. We next examined which subpopulations of fibroblasts expressed sFRP2 in fibrotic lungs.

Sfrp2 expression was found in several subpopulations of fibroblasts within the alveolar compartment as indicated by superimposition of *sfrp2* expression on various feature plots within the alveolar and pathological fibroblast clusters (Figure 2) from untreated or EGCG treated patients (Figure 4C, Supplemental Figure 4B). Virtually all of the *sfrp2* expression co-localized with *col1a1* (Supplemental Figure 4B) and partially with *cthrc1* and the inflammatory marker *ccl2*, all of which were suppressed by EGCG treatment. Although there was little co-localization of *sfrp2* and the alveolar fibroblast markers *inmt* and *tcf21*, the expression of these markers were also obviously suppressed in fibroblasts of EGCG-treated patients (Supplemental Figure 4B). The overall intensity of *sfrp2* signal by in situ hybridization within the alveolar space was substantially decreased in EGCG-treated patients (Figure 4D, E), consistent with the sc-RNA

expression data (Figure 2D). To further define the spatial distribution of *sfrp2* expression, we measured the average distance from *sftpc*+ cells to *sfrp2*+ cells using in situ hybridiztion and found clusters of *sfrp2*$^+$ cells (red) to be substantially correlated with proximity to *sftpc*$^+$ AEC2s and *krt17*$^+$/*sftpc*$^+$ alveolar-basal intermediate (ABIs) cells (Supplemental Figure 5A, B). Finally, we confirmed the reduced expression of sFRP2 by Western-blot protein analysis of precision-cut lung slices from six IPF explants cultured without or with EGCG for 7 days. EGCG effected marked decreases in fibroblast (periostin, sFRP2) and epithelial (KRT17) genes that are upregulated in IPF, as well as increased surfactant protein C (SFTPC) expression (Figure 4F-G, Supplemental Figure 5C).

sFRP2 is an interesting protein relevant to pulmonary fibrosis in several respects. Prior studies have found that sFRP2 is a fibroblast specific protein and its expression increases with age (16, 18). sFRP2 has been linked to fibrosis in several experimental systems (19-21). Interestingly, sFRP2 is found in gene signatures of IPF patients analyzed by GWAS or other linkage analyses (22, 23), suggesting a role in IPF pathobiology. Collectively these findings and the findings detailed above prompted us to explore the functional effects of fibroblast sFRP2 expression *ex vivo*.

SFRP2 induces expression of basal genes in cultured human AEC2 cells. We first tested the impact of recombinant sFRP2 on the fate of AEC2s in organoid co-cultures with the embryonic fibroblast MRC5 as feeder cells, as prior work has established these co-cultures maintain the integrity and support expansion of AEC2 colonies (8). Low concentrations of sFRP2 (10 ng/ml) supported AEC2 integrity with SFTPC expression whereas progressively higher concentrations effected transdifferentiation of the AEC2 cells to KRT5$^+$ basal-like cells (Figure 5A). By day 14 of the co-culture, all the organoids derived from AEC2–MRC5 treated with 60 ng/ml of sFPRP2 contained KRT5$^+$ cells, with some cells still expressing SFTPC,

whereas all the organoids in the AEC2–MRC5 co-culture treated with 10 ng/ml of sFRP2 contained $SFTPC^+$ cells with few expressing KRT5 (Figure 5B and Supplemental Table 4A). Treatment with 30 ng/ml induced an intermediate phenotype, with a similar distribution of cells still expressing SFTPC and cells expressing KRT5 (Figure 5A-B). Given the consistent promoting effects of exogenous sFRP2 on AEC2 transdifferentiation, we asked whether fibroblast expression of sFRP2 was required for fibroblast-dependent expression of KRT5 in AEC2s in cultured organoids. The expression of sFRP2 in primary adult human lung mesenchyme (AHLM) was silenced immediately prior to formation of organoids, as AHLM is known to drive basal metaplasia of AEC2s in coculture organoids (10). We confirmed silencing of *sfrp2* in AHLM transfected with *sfrp2* small interfering (si)RNA vs control siRNA (0.22 ± 0.1 fold expression vs control). *sfrp2* silencing markedly attenuated both loss of SFTPC and gain of KRT5 protein levels in AEC2s in coculture organoids, as compared to organoids formed with AHLM treated with control siRNA (Figure 5C and Supplemental Table 4B). However, some colonies developed mixed phenotypes, comprised of both $SFTPC^+$ and $KRT5^+$ cells, whereas others were virtually devoid of a KRT5 transition (Figure 5C, D). These findings confirm a critical role of mesenchymal sFRP2 in regulating AEC2 cell fate.

To confirm that sFRP2 treatment promoted basaloid differentiation, we isolated RNA from 14-day organoids similar to that shown and quantified mRNA for *krt5*, *ngfr, axin2, and sftpc*. As shown in Figure 5E, sFRP2 promoted *krt5 and ngfr* mRNA expression and decreased *axin2* and sftpc mRNA levels. By 21 days, sFRP2 induced high levels of ngfr, tp63, and krt17 (Figure 5F). Collectively, sFRP2 reduced canonical Wnt signaling and promoted transdifferentiation of AEC2 to basal-like cells.

As a second approach, precision cut lung slices (PCLS) were prepared from non-diseased donor lungs and cultured without or with sFRP2 for 7 days to investigate its effect on basal gene

expression in AEC2s. No KRT5 or KRT17 expression was observed on freshly fixed non-diseased lung section (data not shown). The addition of TGFβ1 (2 ng/mL) promoted the expression of KRT17 in AEC2s, as well as an elongated epithelial morphology by day 3 (not shown) that persisted through day 7 but little or no KRT5 (Figure 5G, H, Supplemental Figure 6). Combined treatment with TGFβ1 and sFRP2 (60 ng/mL) induced a strong expression of KRT5 detected by both western blot analysis of lung slices and immunostaining in very elongated Krt17+ cells by immunofluorescent staining (Figure 5G, H, Supplemental Figure 6). The insert reveals co-localization of KRT17 and KRT5 in elongated AEC2-derived alveolar cells consistent with basal cell cytoplasmic extensions (24). Furthermore, treatment with EGCG reduced the expression of KRT17 and KRT5 suggesting that TGFβ1 promotes KRT17 expression indirectly through the mesenchyme because EGCG does not inhibit TGFβ1 signaling in epithelial cells (11).

sFRP2 acts directly on AEC2s through the Frizzled 5 receptor to activate noncanonical Wnt signaling and promote basal genes expression. To determine whether sFRP2 directly acts on AEC2, we cultured freshly-isolated human AEC2 cells on top of Matrigel without fibroblast support. Because sFRP2 suppressed the canonical Wnt target *axin2* in organoids (Figure 5C) we compared the effects of sFRP2 and Wnt3a on *axin2* levels of cultured AEC2s (Figure 6A). As expected, sFRP2 suppressed whereas Wnt3a induced *axin2* mRNA expression in isolated AEC2s, confirming that sFRP2 does not promote detectable canonical Wnt signaling in these cells. Immunofluorescent staining of parallel AEC2 cell cultures showed that exposure to sFRP2 (60ng/ml) caused loss of SFTPC and induction of $KRT5^{+}$ in AEC2s (Supplemental Figure 7A). Furthermore, qPCR analysis indicated that sFRP2 exposure both induced *krt5* and suppressed *axin2* mRNA (Supplemental Figure 7B). These findings indicate that sFRP2, which

is induced in fibroblasts by TGFβ1, acts directly on AEC2 cells to promote their trans-differentiation toward basal-like cells in organoid co-cultures.

To explore potential receptors for sFRP2 on AEC2s, we examined Frizzled receptor and co-receptor expression in our epithelial scRNA data (Figure 6B). Frizzled 5 (Fzd5) is the Frizzled with highest expression in AEC2s but Fzd6 is the most expressed Frizzled receptor in basal cells. As sFRP2 was recently reported to bind to human endothelial FZD5 receptors and promote non-canonical signaling through a calcineurin/NFAT signaling pathway (25), a similar process may occur in human AEC2s. We therefore tested the role of FZD5 in sFRP2-induced basal gene expression in AEC2s by knocking down *fzd5* via small-interfering RNA and culturing on top of Matrigel with sFRP2 (60 ng/ml). *fzd5* knockdown in AEC2s almost completely blocked the induction of *krt5* mRNA expression by sFRP2, while *fzd6* knockdown did not have significant effect (Figure 6C). Although not statistically significant, the trend toward reduced *krt5* mRNA after *fzd6* knockdown may reflect the switch in relative levels of FZD5 and FZD6 during differentiation of AEC2s toward basal cells (Figure 6B). Knockdown was confirmed in transfected AEC2s as siRNA against *fzd5* reduced its expression to 0.37 ± 0.14 fold relative to control and siRNA against *fzd6* reduced its expression to 0.46 ± 0.07 fold relative to control.

To further test the role of non-canonical Wnt signaling as the mechanism of sFPR2-induced basal gene expression, we examined the effects of two mechanistically distinct inhibitors of the Ca^{2+} activation arm of non-canonical Wnt signaling: KN93, a CaM kinase II inhibitor, and Tacrolimus (26). KN93 blocked upregulation of *krt5* mRNA and downregulation of *axin2* mRNA in 2D cultures of AEC2s stimulated with sFRP2 (60 ng/ml) (Figure 6D). Similarly, Tacrolimus, a direct inhibitor of calcineurin activity, completely blocked sFRP2-induced *krt5* expression and restored *axin2* levels to that of untreated control (Figure 6E). Because dephosphorylation of

NFAT by calcineurin is the key step that promotes its nuclear accumulation and signaling we attempted to demonstrate nuclear NFAT in sFRP2-stimulated primary AEC2 cells. However, we found the basal levels of NFATC3 (the major form of NFAT in human AEC2s) to be low and we were unable to detect nuclear NFAT biochemically. We therefore turned to HEK293 cells which have higher basal NFATC3 and importantly no expression of FZD5. We observed that sFRP2 in three independent experiments induced nuclear NFATC3 accumulation and this was completely dependent on prior transfection of the cells with FZD5 cDNA, confirmed by Western blotting (Figure 6F). A schematic summarizing the effect of sFRP2 on AEC2 cell fate through FZD5 signaling and calcineurin-dependent NFAT nuclear accumulation is shown in Figure 6G and the graphical abstract.

Discussion

Extensive evidence implicates TGFβ1 signaling as a causative driver of fibrotic processes including IPF and other fibrotic ILDs. The findings reported here confirm at a transcriptional level our prior finding demonstrating that selective inhibition of fibroblast TGFβ1 signaling by EGCG attenuates pro-fibrotic signaling at a protein level. We find robust evidence for decreased TGFβ1 signaling due to EGCG, based on changes in expression of individual genes known to be linked to TGFβ1 signaling and by gene pathway analyses. The findings also provide new insights relevant to the mechanisms underlying fibrotic ILDs. Variable TGFβ1 signaling activity in ILD patient tissues at different disease stages has not previously been reported, and suggest that TGFβ1 may have a different effect in patients with mild disease as compared to late or end-stage disease. This is consistent with evidence that matrix accumulation per se can become a TGFβ1-independent driver of more matrix accumulation, in part perhaps related to activation of YAP/TAZ signaling (27, 28). We cannot distinguish between the possibility that TGFβ1 activation and downstream signaling diminishes with late stage disease and the possibility that

this is mainly relative to matrix-dependent signals and infiltration of inflammatory cells that become more robust as disease progresses. In either case, our data suggest that fibroblast TGFβ1 activity may have an especially important role in the development of early tissue-level changes. Further study will be needed to better understand how TGFβ1 activity and other signaling pathways contribute to distinct phases of IPF pathology. This may well impact the choice and testing of drugs to attenuate disease progression.

A surprising finding in our studies is the suppression of epithelial proinflammatory and stress signaling by selective inhibition of fibroblast TGFβ1 signaling. While IPA identified upregulation of many inflammatory pathways in fibroblasts and epithelial cells from untreated biopsy patients and their inhibition by EGCG, it is important to note that these pathways share some common downstream effector mechanisms, which suggest a network of overlapping feed-forward interactions, rather than multiple pathways acting, or inhibited, in isolation. Nonetheless, the overall outcome of EGCG exposure appears to attenuate the activity of multiple proinflammatory and stress effectors and thereby to promote the maintenance of AEC2 differentiation. This conclusion is independently supported by our finding that EGCG reduced KRIT17 (a basaloid cell marker) and increased SFTPC protein in lysates of 5 day PCLS cultures derived from IPF patient explants (Figure 4). What are the underlying mechanisms? One possibility is that EGCG has unrecognized effects on inflammatory signaling pathways identified here, either as a result of, or in addition to, its known inhibition of TGFβ1. However, we favor the view that EGCG effects on the epithelium can mainly be explained by its suppressing secreted fibroblast pro-fibrotic mediators that target the epithelium, e.g. TGFβ1 itself, extracellular matrix proteins, and others implicated in the NicheNet analysis (Figure 3D, E), and by our findings here with sFRP2.

sFRP2 structurally resembles the ectodomain of a Frizzled receptor and was originally identified as a Wnt antagonist (29, 30), presumably by acting as a decoy for Wnt ligand binding. Subsequently, positive effects of sFRP2 on canonical Wnt signaling have been identified (31), and sFRP2 has been found to interact with FZD5 and FZD7 to promote noncanonical Wnt activity (25, 32). Canonical Wnt activity has been repeatedly linked to maintenance of AEC2 fate (33, 34), but is also known to be increased in IPF (35, 36) despite AEC2 loss. sFRP2 expression has previously been linked to TGFβ1 signaling in colonic cancer fibroblasts where inhibition of PKCdelta expression by TGFβ1 induced cell autonomous Sox2 expression and subsequent direct upregulation of sFRP1 and sFRP2 (37). However, in primary normal human lung fibroblasts TGFβ1 selectively induces sFRP2 and not sFRP1 (Supplemental Figure 4A), suggesting different regulation. It remains to be defined whether SOX2 is also involved in this process. In any case, in the human lung fibroblast system studied here sFRP2 does not induce canonical Wnt signaling when compared with Wnt3a (Figure 6A) but promotes the non-canonical FZD5 Ca^{2+} signaling pathway (Figure 6).

Our studies of AEC2-fibroblast coculture organoids and precision cut lung slices (PCLS) (Figure 5G, F) exposed to TGFβ1 without or with sFRP2 shed new light on the process of AEC2 cell transdifferention to basal cells, a prominent feature of human fibrotic lung diseases (38). We find that TGFβ1 signaling alone promotes a spread, AEC2-derived $SFTPC^{-}$/ $KRT17^{+}$ basaloid state, perhaps to cover denuded alveolar walls as recently suggested by studies of AT1 deletion in mice (39). This finding also indicates uncoupling of Krt17 and Krt5 expression, the staged maturation and requirement for additional signaling suggesting a distinct and likely transient function of basaloid cells in alveolar repair. Whether AEC2-derived basal cells, and persistent basaloid cells, become pathological or are themselves capable of resuming an AEC2 or AEC1 state requires further study (7, 40).

There are limitations to this study. The number of patient samples processed and analyzed is small, though the total cells profiled in each group provided substantial statistical power and we were unable to find evidence that variation among individual samples was responsible for our findings. Another limitation is that while we are able to link sFRP2 signaling through FZD5 to calcineurin and nuclear NFAT in a new pathway to basal cell differentiation, we have no evidence for a direct connection between nuclear NFAT and activation of the basal cell transcriptional state. Thus we are uncertain how the NFAT signaling evolves to activate mature basal cell reprogramming. Further elucidation of this pathway will require more study. Finally, an additional limitation is the lack of capture of immune cells from the biopsy samples for sc-RNA sequencing, thereby precluding any assessment of TGFβ1-mediated changes in fibroblast inflammatory markers on the immune system.

In summary, in this manuscript we confirm the central role of TGFβ1 signaling in ILD, finding elevated levels in patients with mild clinical disease. We confirm inhibition of TGFβ1 signaling by EGCG and found multiple downstream likely beneficial effects, such as reduced profibrotic signaling in fibroblasts and reduction in IPF-associated changes in AEC2s. We identify a new fibroblast-dependent pathway required to promote epithelial metaplasia prominent in IPF pathobiology. These results support a potential therapeutic role for EGCG in IPF, which is relevant as there is now active Phase 1/2 trial in IPF patients (ClinicalTrials.gov identifier NCT05195918). Improved treatment in IPF is a pressing clinical need.

Methods

Human Lung Tissue. Tissue from normal lungs declined for transplantation and from IPF patients undergoing transplantation were deidentified and donated to research through institutional protocols approved by the UCSF Institutional Review Board. Patients from the UCSF Interstitial Lung Disease Clinic who were referred for diagnostic surgical lung biopsy were identified and enrolled in a convenience cohort; they took 600mg of EGCG by mouth once daily for two weeks prior to biopsy, and spare biopsy was obtained at the time of surgical resection. Note that for control biopsy 3, FACS-purification of fibroblasts yielded few cells for unclear reasons, so scRNA-seq on this sample was only performed on epithelial cells. Overall, sex was not considered as a biological variable.

Lung tissue processing and fluorescence activated cell sorting.

Lung digestion, fluorescence activated cell sorting (FACS). A single cell preparation of normal, ILD explant, or biopsy tissues was made using mechanical disruption and enzymatic digestion (dispase,15 I.U. ml^{-1}, and collagenase, 225u/ml), as previously described (10). For AEC2 isolation, FACS was performed on digested donor lung tissue for live $EPCAM^{+}/CD11b^{-}/CD31^{-}/CD45^{-}/HT_2\text{-}280^{+}$ cells. For samples used in scRNA-seq, FACS was performed on digested lung tissue for live epithelial ($EPCAM^{+}/CD11b^{-}/CD45^{-}/CD31^{-}$) and mesenchymal ($EPCAM^{-}/CD11b^{-}/CD45^{-}/CD31^{-}$) cells, which were combined 1:1 for processing with the 10x Genomics Chromium platform and sequenced on an Illumina NovaSeq 6000 machine.

Single-cell RNA analysis.

Raw sequencing results were processed with the 10x Genomics Cell Ranger pipeline and analyzed with Seurat version 4, including normalization with SCTransform v2 and integration with the FastMNN packages (41-43). All cells from each sample were initially integrated, followed by iterative subsetting. Clustering was performed by increasing the resolution until differences were not biologically meaningful and then cell annotation was performed using

previously described markers (7, 8, 10, 14-17). Corrected gene counts were used for Feature and Violin Plots. Seurat object cell composition was analyzed in samples containing 500 or more cells. Differential gene expression was performed on SCTv2-normalized counts using the Model-based Analysis of Single-cell Transcriptomics (MAST) method (44). Ingenuity Pathway Analysis (45) was done on differentially-expressed genes using $\log_2$ fold change thresholds of ± 0.25 and adjusted p-values less than 0.05. Single-cell pathway activity analysis was done using the UCell package (46) with MSigDb gene sets (47). Comparative receptor-ligand signaling analysis was performed with NicheNet (48) using normalized RNA counts.

In vitro and *ex vitro* models

Cell culture. MRC5 fibroblasts (Cat#CCL-171, ATCC) and adult human mesenchymal cells were cultured in DMEM (Cat#11965092, Thermo Fisher) with 10% fetal bovine serum (Cat#SH883IH2540, Fisher Scientific), 1% glutamax (Cat#35050-61, Gibco), 1% hepes (Cat#5630-080, Gibco), and 1% Pen/Strep (Cat#10378016, Gibco) . Cells were used within the first five passages of either being received from ATCC for MRC5 cells or being isolated from donor lungs for mesenchymal cells. Where applicable, TGFβ1 (Cat#100-21, Peprotech, 1 and 4 ng ml^{-1}) and SB431442 (Cat#1614/1, Tocris, 5mM), a TGFβ1 inhibitor (49). Where applicable, sFRP2 (Cat#6838-FR, R&D Systems, 60 ng ml^{-1}), Tacrolimus (Cat#AAJ6357AMF, ThermoFisher, 1μM), Wnt3a (Cat#5036-WN-010, R&D, 100ng ml^{-1}), and KN93 (Cat#422711-1MG, MilliporeSigma, 1μM) was added to the medium after 24 hours for 48 hours.

Small-interfering RNA. siRNA probes targeting *sfrp2* in human mesenchymal cells and *frizzled-5* and *-6* in AEC2 cells were obtained from Thermo Fisher (Supplemental Table 5). In brief, 20,000 hAEC2 were incubated for 4 hrs in Opti-DMEM (Cat#31985062, Fisher Scientific) with 1pmole of siRNA probes using Lipofectamine RNAiMAX (Cat#13778, Invitrogen). Cells were then plated on growth factor-reduced Matrigel (Cat#CB-40230A, Thermo Fisher) cultured in

small airway basal medium (SABM Cat#CC-3118, Lonza) with BPE low protein, insulin, transferrin, retinoic acid, epinephrin, triiodothyronine, and epidermal growth factor as per the SAGM bullet kit (Cat#CC-3118, Lonza) supplemented with KGF (Cat#251KG01050, R&D, 100 ng ml^{-1}), 5% charcoal treated FBS (Cat#12676011, ThermoFisher) and 1% Pen/Strep for 48 hrs.

Organoid assay. AEC2s and MRC5 fibroblasts or mesenchymal cells with or without silenced *sfrp2* were co-cultured (5,000 AEC2s: 30,000 fibroblasts/mesenchymal cells per well) in modified MTEC medium diluted 1:1 in growth factor-reduced Matrigel (Cat#CB-40230A, Thermo Fisher). Modified MTEC culture medium is composed of SABM with insulin, transferrin, bovine pituitary extract, retinoic acid and epidermal growth factor (EGF) as per the SAGM Bullet Kit and 0.1 µg ml^{-1} cholera toxin (Cat#C8052, Sigma), 5% charcoal treated FBS and 1% Pen/Strep. The cell suspension–Matrigel mixture was placed in a transwell and incubated with 10 µM ROCK inhibitor (Cat#72252, Stemcell) for the first 24 h. Each experimental condition was performed in triplicate. Where applicable, sFRP2 (10, 30 or 60 ng ml^{-1}), was added to the medium after 24 h and replenished in every medium change. Organoids were processed for OCT-embedding for immunostaining or made into a single cell preparation and positively selected for Epcam for RNA extraction.

Precision Cut Lung Slices. Fresh lung tissues were obtained from normal donors and from IPF patients that underwent lung transplantation. Precision-cut lung slices (PCLS) were prepared as described (12). Lung tissues were inflated with warm 2% low-melting agarose (Cat#16550100, ThermoFisher) and placed in cold PBS. Solidified tissues were cut into 400µm thick slices using Compresstome (Cat#VF-310-0Z; Precisionary Instrument LLC.) One randomly selected slice per well in a 24-well plate were cultured in serum-free DMEM (Dulbecco's modified Eagle's medium) supplemented with 100 units/mL penicillin and streptomycin under standard cell

culture conditions (37 °C, 5% CO2, 100% humidity) with Nystatin (Cat#N186, ThermoFisher, 20U.ml^{-1}. Where applicable, TGFβ1 (2 ng ml^{-1}) and sFRP2 (60 ng ml^{-1}), were added to the medium and replenished in every medium change. At day 5 or 7, all cultured PCLSs were immediately transferred into liquid nitrogen and subsequently stored at −80 °C prior to protein extraction.

Immunofluorescence and In Situ Hybridization.

Paraffin embedding. Diagnosis-biopsy from patients were fixed in 4% paraformaldehyde (PFA) overnight at 4 °C. The lungs were then washed with PBS four times for 30 minutes each at 4 °C, then dehydrated in a series of ethanol (30%, 50%, 70%, 95% and 100%). The dehydrated lungs were incubated with xylene for 1 hour, then embedded in paraffin. The lungs were sectioned at 8 µm on a microtome.

Optimal Cutting Temperature (OCT) embedding. Lungs inflated with 94%OCT/2%PFA/4%PBS and Organoids in 3D Matrigel were fixed with 4% PFA for 1 hour, washed with PBS three times and embedded in OCT after 30% and 15% sucrose gradient washing. Sections (8-µm) were cut on a cryostat.

Immunofluorescent staining. OCT-embedded slides were fixed in 4% PFA for 10 minutes, then washed with PBS. Antigen retrieval (cat. no. DV2004MX, Biocare) was performed for 20 minutes at 95 °C or at 155 °C and washed in distilled water. Slides were washed with PBS, blocked/permeabalized (5% horse serum 0.5% BSA 0.1% Triton X) for 1 hour, and then incubated with primary antibodies overnight at 4 °C (Supplemental Table 6). Slides were washed with PBS and then incubated with secondary antibodies for 1 hour (Supplemental Table 6). 4′,6-Prior to mounting, diamidino-2-phenylindole (DAPI) was added for 5 min and slides were mounted with prolong gold. Images were captured using ZEN v3.1 software (Zeiss). Where

indicated, multiple images at ×20 were captured using the 'MosaiX' function and stitched together using the 'Tile Stitch' function in ZEN.

In Situ Hybridization: Seven μm sections were made from formalin-fixed paraffin-embedded tissue blocks and used for RNAscope fluorescent multiplex assay v2 (Cat#323110 ACDBio) according to manufacturer protocol. Briefly, protease treatment was performed followed by hybridization of probes against SFTPC (Cat#452561, ACDBio), COL1A2 (Cat#432721, ACDBio), KRT17 (Cat#463661 ACDBio) and SFRP2 (Cat#476341, ACDBio) mRNAs (Supplemental Table 5).

Gene expression analysis.

Single cell preparation from organoids and AEC2-2D. The cell–Matrigel mixture in the transwell was washed with PBS and incubated in the 15u/ml dispase for 30-45 mins at 37 °C with intermittent resuspension. The mixture was removed from the transwell and resuspended in TrypLE (Cat#12563011, ThermoFisher). Cells were shaken at 37 °C for up to 20 min, pipetting up and down 10 times every 5 mins and checked for single cells, stained with biotin anti-CD326 (Cat#324216, BioLegend) for 30 min at 4 °C. Streptavidin beads (Cat#17663, STEMCELL) were added to isolate the epithelial cells, and the rest of the cells were mesenchymal cells. AEC-2D cells were washed twice with PBS. Dispase (15U/ml) was added, and plate was incubated for 35 mins shaking at 37 °C. Dispase was carefully collected from the wells without disturbing the matrigel. Wells were washed twice with PBS to ensure recover of all cells.

RNA extraction. RNA was extracted using the ReliaPrep RNA Cell Miniprep System (Cat#Z6011, Promega) as per manufacturer instructions.

Quantitative RT-PCR. Reverse transcription was performed with iScript RT Supermix (Cat#1708841 Bio-Rad) and quantitative real-time PCR (qPCR) was performed using SsoAdvanced Univ SYBR Green Suprmix (Cat#1725271 Biorad). Relative expression was calculated with the delta-delta method. List of primers is provided in Supplemental Table 4.

Protein expression.

Pulverized PCLS tissues were lysed in RIPA buffer and analyzed by immunoblotting as previously described (12). Densitometry was quantified using NIH ImageJ software. List of antibodies is provided in Supplemental Table 6.

293 cell culture and transfection

293 cells (Cat#CRL1573, ATCC) were cultured in DMEM supplemented with penicillin/streptomycin, and 10% FBS. All the cell lines in the laboratory are periodically tested for mycoplasma contamination. Only the mycoplasma-free cells are used for experiments. For transfection, 293 cells with 80% confluency were co-transfected with FZD plasmid (GenScript) using TurboFect transfection reagent (Cat#R0531, Thermo Fisher) and cultured in DMEM complete medium for 24-48 hours. Cells were washed with PBS for 3 times and replaced with serum-free medium with or without SFRP2 (30 ng ml^{-1}) for 1 hour at 37 °C before lysis for nuclei isolation.

Isolation of nuclei

293 cells transfected with FZD5 were lysed in ice-cold NP40 lysis buffer (5 mm Tris, pH 8.0, 15 mm NaCl, and 0.1% NP40) supplemented with protease/phosphotase inhibitors and 1 mm phenylmethylsulfonyl fluoride. After 5 minutes incubation with lysis buffer, cells were scaped off and centrifuged at 500 g for 5 minutes at 4 °C. Supernatant was saved as cytosol control. Nuclei pellet was washed with lysis buffer once before solubilizing in RIPA buffer. Clarified nuclei

supernatant along with cytosol control were blotted for NFAT3 (Cat#sc8405, Santa Cruz), FZD5 (Cat#MA5-17080, ThermoFisher), GAPDH (Cat#sc-47724, Santa Cruz), or NUP62 (Cat#13916-AP, ThermoFisher).

Image quantification.

Sections were imaged for quantification on a Zeiss AxioImager.M1 microscope. Cell counts for stained organoids were performed manually. Approximatively 1,000 cells per condition were counted. The results were averaged between each specimen and s.d. values were calculated per condition. For RNAscope images, nuclei (dapi) were used to locate and identify individual cells. To avoid overlapping nuclei, area, circularity and intensity range are restricted (28.639 ~ 154.142 μm2 ; 0.644 ~ 0.883; gray level 41.00 ~ 1907.00, respectively). Signals (SFTPC, GFP; sFRP2, RFP) that overlapped with nuclei were counted as positive. Coordinate of positive cells were then measured by center of nuclei to X-axis and Y-axis. sFRP2+ cells to SFTPC+ cells direct distance calculated by $\sqrt{(x2 - X1)^2 + (Y2 - Y1)^2}$. For the quantification in biopsies, the level of expression of sFRP2 was measured as the highest value in the largest area in the look-up table (LUT).

Statistics.

Statistical analysis of scRNA-seq gene expression was performed in Seurat with MAST. Overlapping gene lists were compared with nemates.org with a base value of 30,000 genes in the genome. Cell composition analysis was done using in Excel with a two-tailed t-test. Statistical analyses for cell count and gene and protein expression were performed in GraphPad Prism. One-Way ANOVA, Unpaired and paired two-tailed t-tests were used to determine the P values, and the data in the graphs are presented as mean ± s.d. Unpaired t-test was used to compare two treatment groups. The Kruskal–Wallis test or Dunnett's multiple comparisons test

were used for multiple comparisons. For normally distributed data, ordinary one-way ANOVA followed by Tukey's multiple comparisons test was performed.

Study approval.

The study protocol for enrollment of ILD patients prior to biopsy into an EGCG-treated vs Control cohorts was reviewed and approved by the UCSF Institutional Review Board, and prospectively entered at ClinicalTrials.gov with identifier NCT03928847.

Data Availability.

RNA-seq data reported in this paper is deposited in NCBI Gene Expression Omnibus (GEO) under the accession number GSE239664. Previously published scRNA-seq data that were included in the analysis include GEO samples GSE135893 and GSE132771. Publicly available R packages were used for all computational analyses. No custom codes were developed. Representative code is available on reasonable request. Data used for graphing/quantification purposes are provided in the Supporting Data Values file. All raw data used for quantification and statistical analysis are available in a single GraphPad Prism file that can be made available upon request.

Author Contributions

MLC, YW, HAC, and CJLS conceived the study. ANB, TCH, YW, KG, MLC, and CJLS performed the experiments. MLC analyzed single-cell RNA transcriptome data. ANB, HAC, TCH, and CJLS analyzed the cell biology data. YW analyzed biochemical data. MLC, GM, DL, JAG, YW, and HAC recruited ILD patients, and BNT and DJ performed surgical lung biopsies. MM , KJ, and PJW provided human lung samples. DL and YW coordinated surgical lung tissue collection. MLC, HAC, and CJLS wrote the manuscript. All authors read and reviewed the manuscript. MLC and ANB were designated co-first authors based on their relative overall contributions to performing and analyzing the bioinformatic and cell biology aspects of the study, respectively. MLC was listed first for his input to the conception of the study.

Acknowledgements

The authors thank the Donor Network West for procuring donor lungs for research. They also thank the UCSF Genomics CoLab for support with single-cell transcriptomics sample preparation and sequencing. This work is supported by NIH grants R35HL150767 and U01HL134766 and California Institute for Regenerative Medicine grant DISC0-13788 (H.A.C.), NIH grants 5T32HL007185 and F32HL156356 (M.L.C.), and by the Nina Ireland Program Award for human lung collection (M.M.). The UCSF Wynton High Performance Computer was used for computational analyses. Biorender was used in figure preparation.

References

1. Wolters PJ, Blackwell TS, Eickelberg O, Loyd JE, Kaminski N, Jenkins G, et al. Time for a change: is idiopathic pulmonary fibrosis still idiopathic and only fibrotic? *The Lancet Respiratory Medicine.* 2018;6(2):154-60.
2. Wijsenbeek M, and Cottin V. Spectrum of Fibrotic Lung Diseases. *New England Journal of Medicine.* 2020;383(10):958-68.
3. Lederer DJ, and Martinez FJ. Idiopathic Pulmonary Fibrosis. *N Engl J Med.* 2018;378(19):1811-23.
4. Katzenstein AL. Pathogenesis of "fibrosis" in interstitial pneumonia: an electron microscopic study. *Human Pathology.* 1985;16(10):1015-24.
5. Myers JL, and Katzenstein A-LA. Epithelial Necrosis and Alveolar Collapse in the Pathogenesis of Usual Interstitial Pneumonia. *Chest.* 1988;94(6):1309-11.
6. Katzenstein AL. Idiopathic interstitial pneumonia: classification and diagnosis. *Monographs in Pathology.* 1993(36):1-31.
7. Adams TS, Schupp JC, Poli S, Ayaub EA, Neumark N, Ahangari F, et al. Single-cell RNA-seq reveals ectopic and aberrant lung-resident cell populations in idiopathic pulmonary fibrosis. *Science Advances.* 2020;6(28):eaba1983.
8. Habermann AC, Gutierrez AJ, Bui LT, Yahn SL, Winters NI, Calvi CL, et al. Single-cell RNA sequencing reveals profibrotic roles of distinct epithelial and mesenchymal lineages in pulmonary fibrosis. *Science Advances.* 2020;6(28):eaba1972.
9. Barkauskas CE, Cronce MJ, Rackley CR, Bowie EJ, Keene DR, Stripp BR, et al. Type 2 alveolar cells are stem cells in adult lung. *J Clin Invest.* 2013;123(7):3025-36.
10. Kathiriya JJ, Wang C, Zhou M, Brumwell A, Cassandras M, Le Saux CJ, et al. Human alveolar type 2 epithelium transdifferentiates into metaplastic KRT5(+) basal cells. *Nat Cell Biol.* 2022;24(1):10-23.

11. Wei Y, Kim TJ, Peng DH, Duan D, Gibbons DL, Yamauchi M, et al. Fibroblast-specific inhibition of TGF-beta1 signaling attenuates lung and tumor fibrosis. *J Clin Invest.* 2017;127(10):3675-88.
12. Wei Y, Dong W, Jackson J, Ho TC, Le Saux CJ, Brumwell A, et al. Blocking LOXL2 and TGFbeta1 signalling induces collagen I turnover in precision-cut lung slices derived from patients with idiopathic pulmonary fibrosis. *Thorax.* 2021;76(7):729-32.
13. Chapman HA, Wei Y, Montas G, Leong D, Golden JA, Trinh BN, et al. Reversal of TGFβ1-Driven Profibrotic State in Patients with Pulmonary Fibrosis. *New England Journal of Medicine.* 2020;382(11):1068-70.
14. Wang C, de Mochel NSR, Christenson SA, Cassandras M, Moon R, Brumwell AN, et al. Expansion of hedgehog disrupts mesenchymal identity and induces emphysema phenotype. *J Clin Invest.* 2018;128(10):4343-58.
15. Tsukui T, Sun K-H, Wetter JB, Wilson-Kanamori JR, Hazelwood LA, Henderson NC, et al. Collagen-producing lung cell atlas identifies multiple subsets with distinct localization and relevance to fibrosis. *Nature Communications.* 2020;11(1):1920.
16. Travaglini KJ, Nabhan AN, Penland L, Sinha R, Gillich A, Sit RV, et al. A molecular cell atlas of the human lung from single-cell RNA sequencing. *Nature.* 2020;587(7835):619-25.
17. Tsukui T, and Sheppard D. Tracing the origin of pathologic pulmonary fibroblasts. *bioRxiv.* 2022:2022.11.18.517147.
18. Kaur A, Webster MR, Marchbank K, Behera R, Ndoye A, Kugel CH, 3rd, et al. sFRP2 in the aged microenvironment drives melanoma metastasis and therapy resistance. *Nature.* 2016;532(7598):250-4.
19. Sun Z, Li S, Cao C, Wu J, Ma B, and Tran V. shRNA targeting SFRP2 promotes the apoptosis of hypertrophic scar fibroblast. *Mol Cell Biochem.* 2011;352(1-2):25-33.

20. Liu Y, El-Serag HB, Jiao L, Lee J, Moore D, Franco LM, et al. WNT signaling pathway gene polymorphisms and risk of hepatic fibrosis and inflammation in HCV-infected patients. *PLoS One.* 2013;8(12):e84407.
21. Xu H, Wang Z, Yang H, Zhu J, and Hu Z. Bioinformatics analysis and identification of dysregulated POSTN in the pathogenesis of keloid. *Int Wound J.* 2023;20(5):1700-11.
22. Gangwar I, Kumar Sharma N, Panzade G, Awasthi S, Agrawal A, and Shankar R. Detecting the Molecular System Signatures of Idiopathic Pulmonary Fibrosis through Integrated Genomic Analysis. *Sci Rep.* 2017;7(1):1554.
23. Ghandikota S, Sharma M, Ediga HH, Madala SK, and Jegga AG. Consensus Gene Co-Expression Network Analysis Identifies Novel Genes Associated with Severity of Fibrotic Lung Disease. *Int J Mol Sci.* 2022;23(10).
24. Shum WW, Da Silva N, McKee M, Smith PJ, Brown D, and Breton S. Transepithelial projections from basal cells are luminal sensors in pseudostratified epithelia. *Cell.* 2008;135(6):1108-17.
25. Peterson YK, Nasarre P, Bonilla IV, Hilliard E, Samples J, Morinelli TA, et al. Frizzled-5: a high affinity receptor for secreted frizzled-related protein-2 activation of nuclear factor of activated T-cells c3 signaling to promote angiogenesis. *Angiogenesis.* 2017;20(4):615-28.
26. Siamakpour-Reihani S, Caster J, Bandhu Nepal D, Courtwright A, Hilliard E, Usary J, et al. The role of calcineurin/NFAT in SFRP2 induced angiogenesis--a rationale for breast cancer treatment with the calcineurin inhibitor tacrolimus. *PLoS One.* 2011;6(6):e20412.
27. Gao A, Diaz Espinosa AM, Nguyen BBN, Link PA, Meridew J, Jones DL, et al. DRD1 is exempt from TGFbeta-mediated antifibrotic GPCR landscape tampering in lung fibroblasts. *J Pharmacol Exp Ther.* 2023.
28. Liu F, Lagares D, Choi KM, Stopfer L, Marinkovic A, Vrbanac V, et al. Mechanosignaling through YAP and TAZ drives fibroblast activation and fibrosis. *Am J Physiol Lung Cell Mol Physiol.* 2015;308(4):L344-57.

29. Rattner A, Hsieh J-C, Smallwood PM, Gilbert DJ, Copeland NG, Jenkins NA, et al. A family of secreted proteins contains homology to the cysteine-rich ligand-binding domain of frizzled receptors. *Proceedings of the National Academy of Sciences.* 1997;94(7):2859-63.
30. Ladher RK, Church VL, Allen S, Robson L, Abdelfattah A, Brown NA, et al. Cloning and Expression of the Wnt Antagonists Sfrp-2 and Frzb during Chick Development. *Developmental Biology.* 2000;218(2):183-98.
31. von Marschall Z, and Fisher LW. Secreted Frizzled-related protein-2 (sFRP2) augments canonical Wnt3a-induced signaling. *Biochem Biophys Res Commun.* 2010;400(3):299-304.
32. Brinkmann E-M, Mattes B, Kumar R, Hagemann AIH, Gradl D, Scholpp S, et al. Secreted Frizzled-related Protein 2 (sFRP2) Redirects Non-canonical Wnt Signaling from Fz7 to Ror2 during Vertebrate Gastrulation*. *Journal of Biological Chemistry.* 2016;291(26):13730-42.
33. Nabhan AN, Brownfield DG, Harbury PB, Krasnow MA, and Desai TJ. Single-cell Wnt signaling niches maintain stemness of alveolar type 2 cells. *Science.* 2018;359:1118-23.
34. Nabhan AN, Webster JD, Adams JJ, Blazer L, Everrett C, Eidenschenk C, et al. Targeted alveolar regeneration with Frizzled-specific agonists. *Cell.* 2023.
35. Chilosi M, Poletti V, Zamo A, Lestani M, Montagna L, Piccoli P, et al. Aberrant Wnt/beta-catenin pathway activation in idiopathic pulmonary fibrosis. *American Journal of Pathology.* 2003;162(5):1495-502.
36. Königshoff M, Balsara N, Pfaff E-M, Kramer M, Chrobak I, Seeger W, et al. Functional Wnt Signaling Is Increased in Idiopathic Pulmonary Fibrosis. *PLOS ONE.* 2008;3(5):e2142.
37. Kasashima H, Duran A, Martinez-Ordonez A, Nakanishi Y, Kinoshita H, Linares JF, et al. Stromal SOX2 Upregulation Promotes Tumorigenesis through the Generation of a SFRP1/2-Expressing Cancer-Associated Fibroblast Population. *Dev Cell.* 2021;56(1):95-110 e10.

38. Xu Y, Mizuno T, Sridharan A, Du Y, Guo M, Tang J, et al. Single-cell RNA sequencing identifies diverse roles of epithelial cells in idiopathic pulmonary fibrosis. *JCI Insight.* 2016;1(20):e90558.
39. Guild J, Juul NH, Andalon A, Taenaka H, Coffey RJ, Matthay MA, et al. Evidence for lung barrier regeneration by differentiation prior to binucleated and stem cell division. *J Cell Biol.* 2023;222(12).
40. Xie T, Lynn H, Parks WC, Stripp B, Chen P, Jiang D, et al. Abnormal respiratory progenitors in fibrotic lung injury. *Stem Cell Res Ther.* 2022;13(1):64.
41. Butler A, Hoffman P, Smibert P, Papalexi E, and Satija R. Integrating single-cell transcriptomic data across different conditions, technologies, and species. *Nat Biotechnol.* 2018;36(5):411-20.
42. Haghverdi L, Lun ATL, Morgan MD, and Marioni JC. Batch effects in single-cell RNA-sequencing data are corrected by matching mutual nearest neighbors. *Nature Biotechnology.* 2018;36(5):421-7.
43. Hafemeister C, and Satija R. Normalization and variance stabilization of single-cell RNA-seq data using regularized negative binomial regression. *Genome Biology.* 2019;20(1):296.
44. Finak G, McDavid A, Yajima M, Deng J, Gersuk V, Shalek AK, et al. MAST: a flexible statistical framework for assessing transcriptional changes and characterizing heterogeneity in single-cell RNA sequencing data. *Genome Biology.* 2015;16(1):278.
45. Krämer A, Green J, Pollard J, Jr, and Tugendreich S. Causal analysis approaches in Ingenuity Pathway Analysis. *Bioinformatics.* 2013;30(4):523-30.
46. Andreatta M, and Carmona SJ. UCell: Robust and scalable single-cell gene signature scoring. *Computational and Structural Biotechnology Journal.* 2021;19:3796-8.
47. Liberzon A, Birger C, Thorvaldsdóttir H, Ghandi M, Mesirov Jill P, and Tamayo P. The Molecular Signatures Database Hallmark Gene Set Collection. *Cell Systems.* 2015;1(6):417-25.

48. Browaeys R, Saelens W, and Saeys Y. NicheNet: modeling intercellular communication by linking ligands to target genes. *Nature Methods.* 2020;17(2):159-62.
49. Katsura H, Sontake V, Tata A, Kobayashi Y, Edwards CE, Heaton BE, et al. Human Lung Stem Cell-Based Alveolospheres Provide Insights into SARS-CoV-2-Mediated Interferon Responses and Pneumocyte Dysfunction. *Cell Stem Cell.* 2020;27(6):890-904 e8.

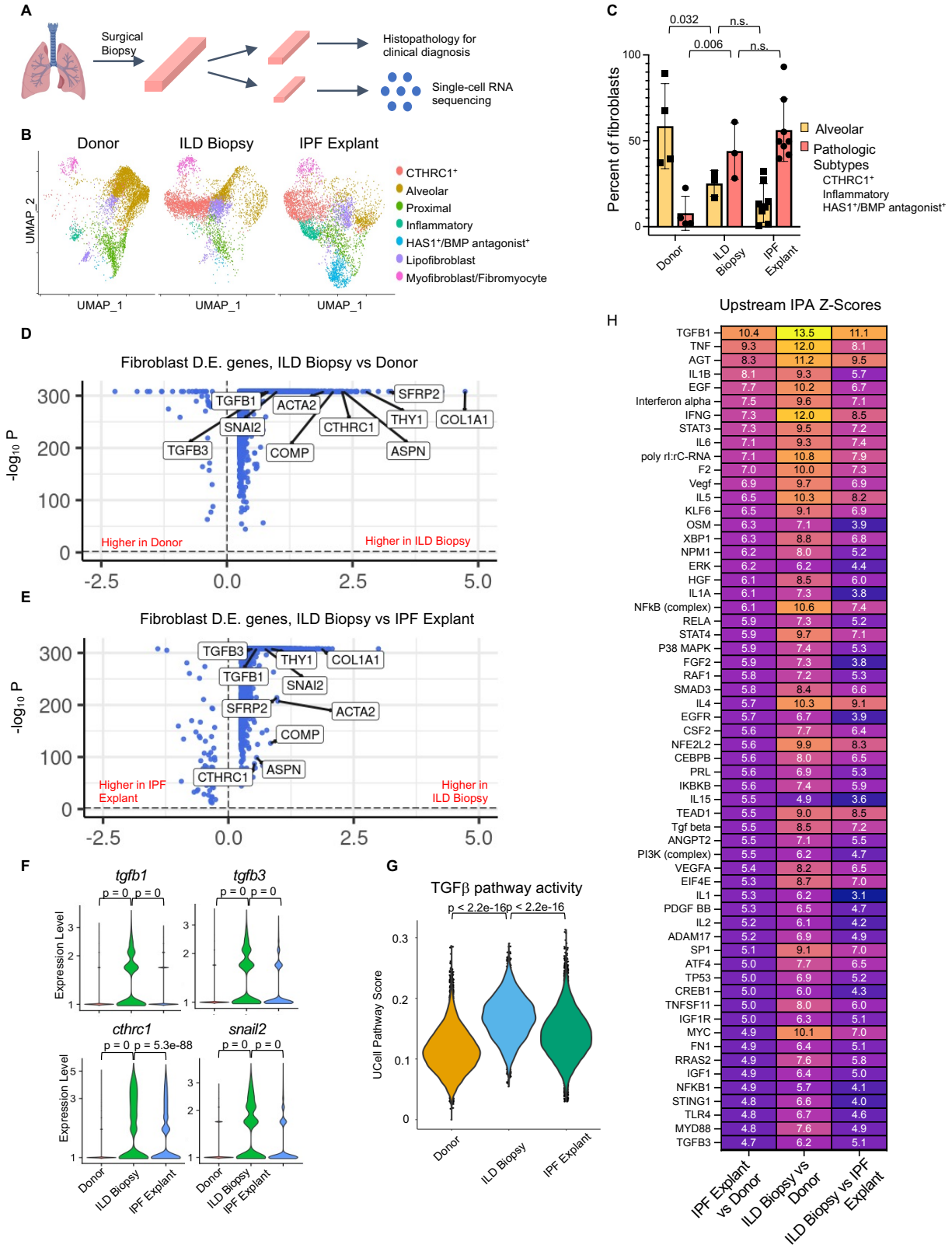
A
Surgical Biopsy
Histopathology for clinical diagnosis
Single-cell RNA sequencing
B
Donor
ILD Biopsy
IPF Explant
UMAP_2
UMAP_1
CTHRC1+
Alveolar
Proximal
Inflammatory
HAS1+/BMP antagonist+
Lipofibroblast
Myofibroblast/Fibromyocyte
C
0.032
n.s.
0.006
n.s.
Percent of fibroblasts
Alveolar
Pathologic Subtypes
CTHRC1+
Inflammatory
HAS1+/BMP antagonist+
Donor
ILD Biopsy
IPF Explant
D
Fibroblast D.E. genes, ILD Biopsy vs Donor
-log10 P
TGFB1
ACTA2
SFRP2
SNAI2
CTHRC1
THY1
COL1A1
TGFB3
COMP
ASPN
Higher in Donor
Higher in ILD Biopsy
E
Fibroblast D.E. genes, ILD Biopsy vs IPF Explant
TGFB3
THY1
COL1A1
TGFB1
SNAI2
SFRP2
ACTA2
COMP
ASPN
CTHRC1
Higher in IPF Explant
Higher in ILD Biopsy
F
tgfb1
tgfb3
cthrc1
snail2
p = 0
p = 5.3e-88
Expression Level
Donor
ILD Biopsy
IPF Explant
G
TGFβ pathway activity
p < 2.2e-16
UCell Pathway Score
H
Upstream IPA Z-Scores
TGFB1 10.4 13.5 11.1
TNF 9.3 12.0 8.1
AGT 8.3 11.2 9.5
IL1B 8.1 9.3 5.7
EGF 7.7 10.2 6.7
Interferon alpha 7.5 9.6 7.1
IFNG 7.3 12.0 8.5
STAT3 7.3 9.5 7.2
IL6 7.1 9.3 7.4
poly rI:rC-RNA 7.1 10.8 7.9
F2 7.0 10.0 7.3
Vegf 6.9 9.7 6.9
IL5 6.5 10.3 8.2
KLF6 6.5 9.1 6.9
OSM 6.3 7.1 3.9
XBP1 6.3 8.8 6.8
NPM1 6.2 8.0 5.2
ERK 6.2 6.2 4.4
HGF 6.1 8.5 6.0
IL1A 6.1 7.3 3.8
NFkB (complex) 6.1 10.6 7.4
RELA 5.9 7.3 5.2
STAT4 5.9 9.7 7.1
P38 MAPK 5.9 7.4 5.3
FGF2 5.9 7.3 3.8
RAF1 5.8 7.2 5.3
SMAD3 5.8 8.4 6.6
IL4 5.7 10.3 9.1
EGFR 5.7 6.7 3.9
CSF2 5.6 7.7 6.4
NFE2L2 5.6 9.9 8.3
CEBPB 5.6 8.0 6.5
PRL 5.6 6.9 5.3
IKBKB 5.6 7.4 5.9
IL15 5.5 4.9 3.6
TEAD1 5.5 9.0 8.5
Tgf beta 5.5 8.5 7.2
ANGPT2 5.5 7.1 5.5
PI3K (complex) 5.5 6.2 4.7
VEGFA 5.4 8.2 6.5
EIF4E 5.3 8.7 7.0
IL1 5.3 6.2 3.1
PDGF BB 5.3 6.5 4.7
IL2 5.2 6.1 4.2
ADAM17 5.2 6.9 4.9
SP1 5.1 9.1 7.0
ATF4 5.0 7.7 6.5
TP53 5.0 6.9 5.2
CREB1 5.0 6.0 4.3
TNFSF11 5.0 8.0 6.0
IGF1R 5.0 6.3 5.1
MYC 4.9 10.1 7.0
FN1 4.9 6.4 5.1
RRAS2 4.9 7.6 5.8
IGF1 4.9 6.4 5.0
NFKB1 4.9 5.7 4.1
STING1 4.8 6.6 4.0
TLR4 4.8 6.7 4.6
MYD88 4.8 7.6 4.9
TGFB3 4.7 6.2 5.1
IPF Explant vs Donor
ILD Biopsy vs Donor
ILD Biopsy vs IPF Explant

Figure 1: Fibroblasts from ILD biopsy have higher TGFβ signaling than fibroblasts from ILD explants.

(A) Schematic of processing diagnostic lung biopsies of ILD patients. **(B)** Dimensional Reduction Plot of fibroblasts from donor (13,856 cells, n = 13), ILD biopsy (7,724 cells, n = 3), and IPF explant (21,192 cells, n = 26) samples. **(C)** Fibroblast subtype composition by sample type. **(D,E)** Volcano plots of differentially expressed (D.E.) genes in all fibroblasts from ILD biopsy samples vs donor samples and ILD biopsy samples vs IPF explant samples, with selected TGFβ-pathway related genes labelled. **(F)** Violin plot of selected TGFβ1 related genes in all fibroblasts. **(G)** Single-cell activity of Hallmark TGFβ pathway in all fibroblasts. **(H)** Heatmap of Z-scores from pairwise upstream Ingenuity Pathway Analysis (IPA) of differentially expressed genes from all fibroblasts. Statistical significance was determined by 2-tailed t-test (C,F,G) and MAST with adjustment for multiple comparisons (D,E).

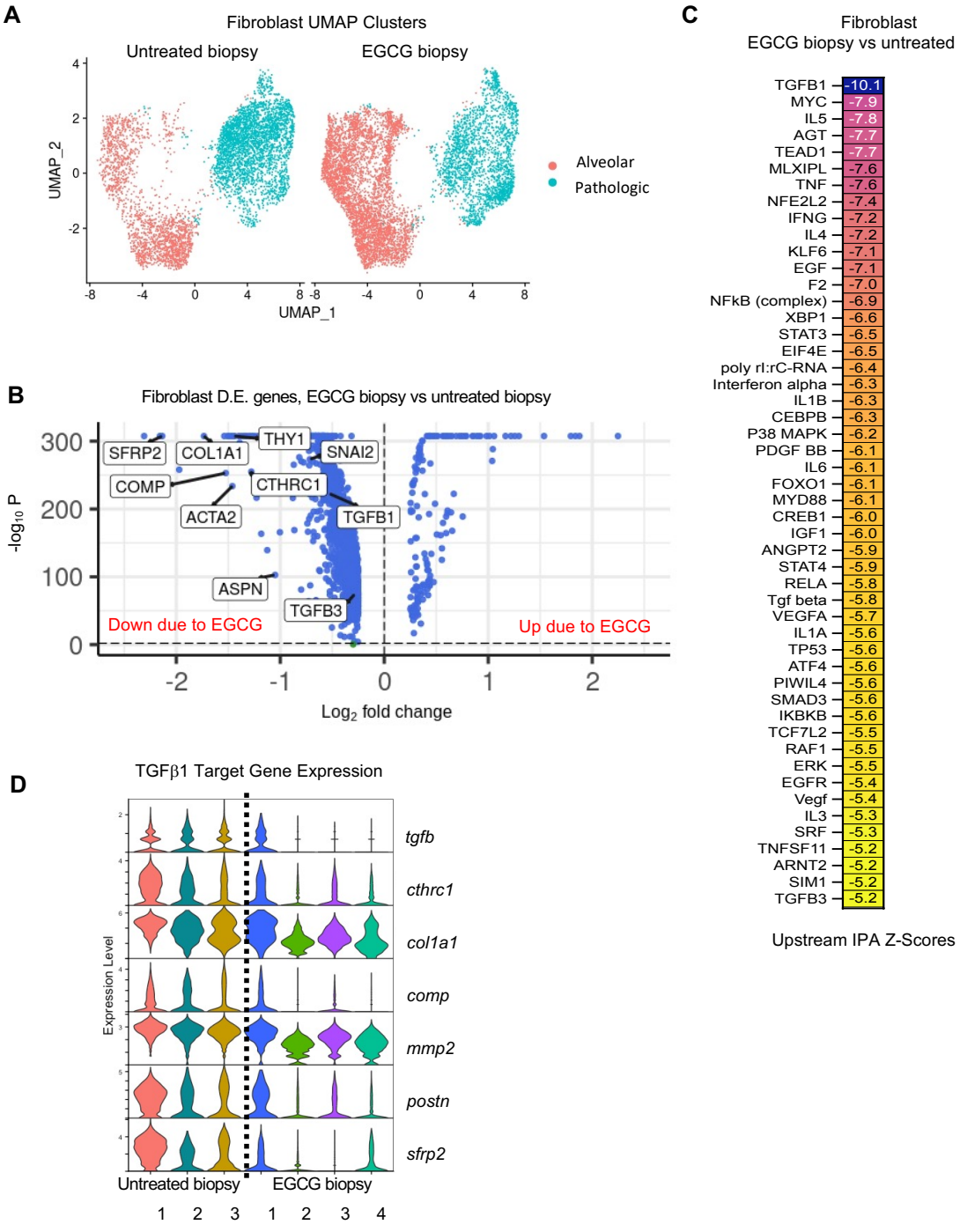
A
Fibroblast UMAP Clusters
Untreated biopsy
EGCG biopsy
UMAP_2
UMAP_1
Alveolar
Pathologic
B
Fibroblast D.E. genes, EGCG biopsy vs untreated biopsy
-log10 P
Log2 fold change
SFRP2
COL1A1
THY1
SNAI2
COMP
CTHRC1
ACTA2
TGFB1
ASPN
TGFB3
Down due to EGCG
Up due to EGCG
C
Fibroblast
EGCG biopsy vs untreated biopsy
TGFB1 -10.1
MYC -7.9
IL5 -7.8
AGT -7.7
TEAD1 -7.7
MLXIPL -7.6
TNF -7.6
NFE2L2 -7.4
IFNG -7.2
IL4 -7.2
KLF6 -7.1
EGF -7.1
F2 -7.0
NFkB (complex) -6.9
XBP1 -6.6
STAT3 -6.5
EIF4E -6.5
poly rI:rC-RNA -6.4
Interferon alpha -6.3
IL1B -6.3
CEBPB -6.3
P38 MAPK -6.2
PDGF BB -6.1
IL6 -6.1
FOXO1 -6.1
MYD88 -6.1
CREB1 -6.0
IGF1 -6.0
ANGPT2 -5.9
STAT4 -5.9
RELA -5.8
Tgf beta -5.8
VEGFA -5.7
IL1A -5.6
TP53 -5.6
ATF4 -5.6
PIWIL4 -5.6
SMAD3 -5.6
IKBKB -5.6
TCF7L2 -5.5
RAF1 -5.5
ERK -5.5
EGFR -5.4
Vegf -5.4
IL3 -5.3
SRF -5.3
TNFSF11 -5.2
ARNT2 -5.2
SIM1 -5.2
TGFB3 -5.2
Upstream IPA Z-Scores
D
TGFβ1 Target Gene Expression
Expression Level
tgfb
cthrc1
col1a1
comp
mmp2
postn
sfrp2
Untreated biopsy
EGCG biopsy
1 2 3 1 2 3 4

Figure 2: EGCG inhibits TGFβ1-pathway activity in fibroblasts from ILD biopsies and identifies sFRP2 as a downstream target gene.

(A) Dimensional Reduction Plot of subsetted and reclustered alveolar (red) & pathologic (blue) (CTHRC1^{+}, Inflammatory, and HAS1^{+}/BMP Antagonist^{+}) fibroblast subtypes from untreated biopsy (5,225 cells, n = 3) and EGCG biopsy (6,773 cells, n = 4) samples. **(B)** Volcano plot of differentially expressed (D.E.) genes in alveolar and pathologic fibroblasts subtypes from EGCG biopsy vs untreated biopsy samples, with selected TGFβ-pathway genes labelled, including sFRP2. **(C)** Heatmap of Z-scores from IPA upstream pathway analysis of differentially expressed genes in alveolar and pathologic fibroblasts subtypes from EGCG biopsy vs untreated biopsy samples. **(D)** Violin plots of selected TGFβ-pathway genes split by individual biopsy sample.

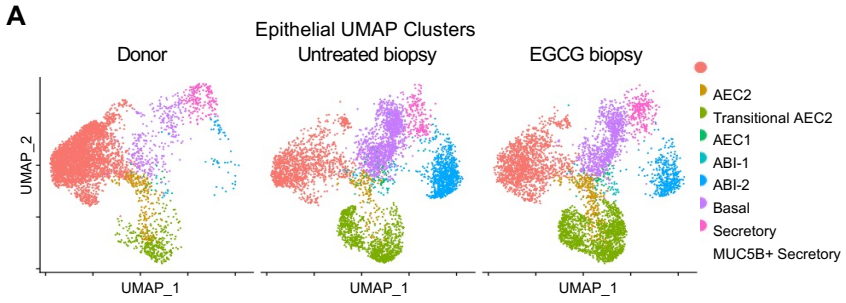
A
Epithelial UMAP Clusters
Donor
Untreated biopsy
EGCG biopsy
UMAP_2
UMAP_1
UMAP_1
UMAP_1
AEC2
Transitional AEC2
AEC1
ABI-1
ABI-2
Basal
Secretory
MUC5B+ Secretory

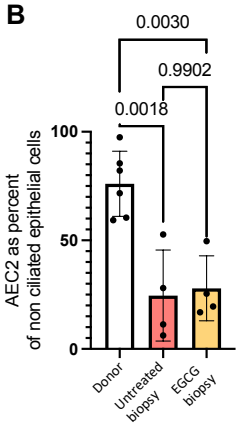
B
0.0030
0.9902
0.0018
AEC2 as percent of non ciliated epithelial cells
100
50
0
Donor
Untreated biopsy
EGCG biopsy

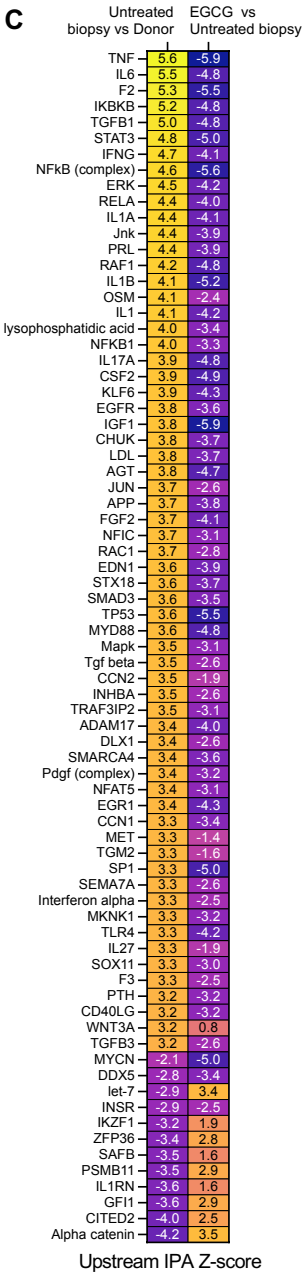
C
Untreated biopsy vs Donor
EGCG vs Untreated biopsy
TNF 5.6 -5.9
IL6 5.5 -4.8
F2 5.3 -5.5
IKBKB 5.2 -4.8
TGFB1 5.0 -4.8
STAT3 4.8 -5.0
IFNG 4.7 -4.1
NFkB (complex) 4.6 -5.6
ERK 4.5 -4.2
RELA 4.4 -4.0
IL1A 4.4 -4.1
Jnk 4.4 -3.9
PRL 4.4 -3.9
RAF1 4.2 -4.8
IL1B 4.1 -5.2
OSM 4.1 -2.4
IL1 4.1 -4.2
lysophosphatidic acid 4.0 -3.4
NFKB1 4.0 -3.3
IL17A 3.9 -4.8
CSF2 3.9 -4.9
KLF6 3.9 -4.3
EGFR 3.8 -3.6
IGF1 3.8 -5.9
CHUK 3.8 -3.7
LDL 3.8 -3.7
AGT 3.8 -4.7
JUN 3.7 -2.6
APP 3.7 -3.8
FGF2 3.7 -4.1
NFIC 3.7 -3.1
RAC1 3.7 -2.8
EDN1 3.6 -3.9
STX18 3.6 -3.7
SMAD3 3.6 -3.5
TP53 3.6 -5.5
MYD88 3.6 -4.8
Mapk 3.5 -3.1
Tgf beta 3.5 -2.6
CCN2 3.5 -1.9
INHBA 3.5 -2.6
TRAF3IP2 3.5 -3.1
ADAM17 3.4 -4.0
DLX1 3.4 -2.6
SMARCA4 3.4 -3.6
Pdgf (complex) 3.4 -3.2
NFAT5 3.4 -3.1
EGR1 3.4 -4.3
CCN1 3.3 -3.4
MET 3.3 -1.4
TGM2 3.3 -1.6
SP1 3.3 -5.0
SEMA7A 3.3 -2.6
Interferon alpha 3.3 -2.5
MKNK1 3.3 -3.2
TLR4 3.3 -4.2
IL27 3.3 -1.9
SOX11 3.3 -3.0
F3 3.3 -2.5
PTH 3.2 -3.2
CD40LG 3.2 -3.2
WNT3A 3.2 0.8
TGFB3 3.2 -2.6
MYCN -2.1 -5.0
DDX5 -2.8 -3.4
let-7 -2.9 3.4
INSR -2.9 -2.5
IKZF1 -3.2 1.9
ZFP36 -3.4 2.8
SAFB -3.5 1.6
PSMB11 -3.5 2.9
IL1RN -3.6 1.6
GFI1 -3.6 2.9
CITED2 -4.0 2.5
Alpha catenin -4.2 3.5
Upstream IPA Z-score

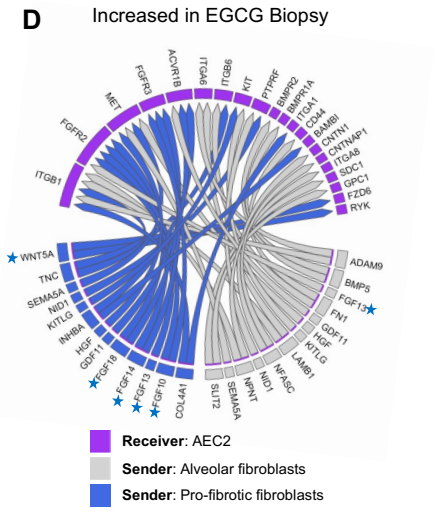
D
Increased in EGCG Biopsy
Receiver: AEC2
Sender: Alveolar fibroblasts
Sender: Pro-fibrotic fibroblasts

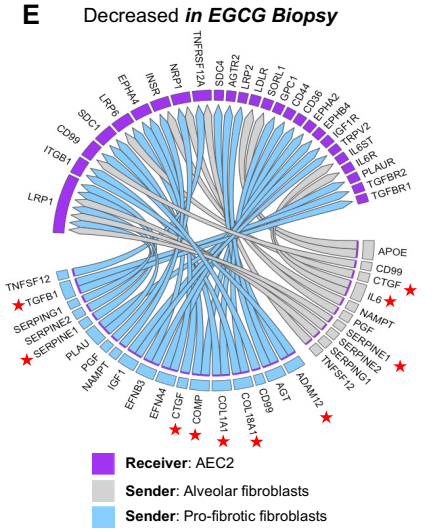
E
Decreased in EGCG Biopsy
Receiver: AEC2
Sender: Alveolar fibroblasts
Sender: Pro-fibrotic fibroblasts

Figure 3: EGCG inhibits IPF-associated changes in biopsy AEC2s

(A) Dimensional Reduction Plot of nonciliated epithelial subtypes from donors (10,127 cells, n = 14), untreated biopsy (10,336 cells, n = 4) and EGCG biopsy samples (11,585 cells, n = 4). **(B)** AEC2s as percent of nonciliated epithelium. **(C)** Heatmap of selected top up- and down-regulated Upstream IPA pathways from untreated biopsy vs Donor and EGCG biopsy vs untreated biopsy comparisons in AEC2s. **(D, E)** NicheNet prediction of differential receptor-ligand signaling from fibroblasts to AEC2s as a result of EGCG. Blue stars highlight AEC2 trophic factors increased in EGCG biopsy samples, and red stars highlight pro-fibrotic pathways decreased in EGCG biopsy samples. Statistical significance was determined by Šídák's multiple comparisons test (B).

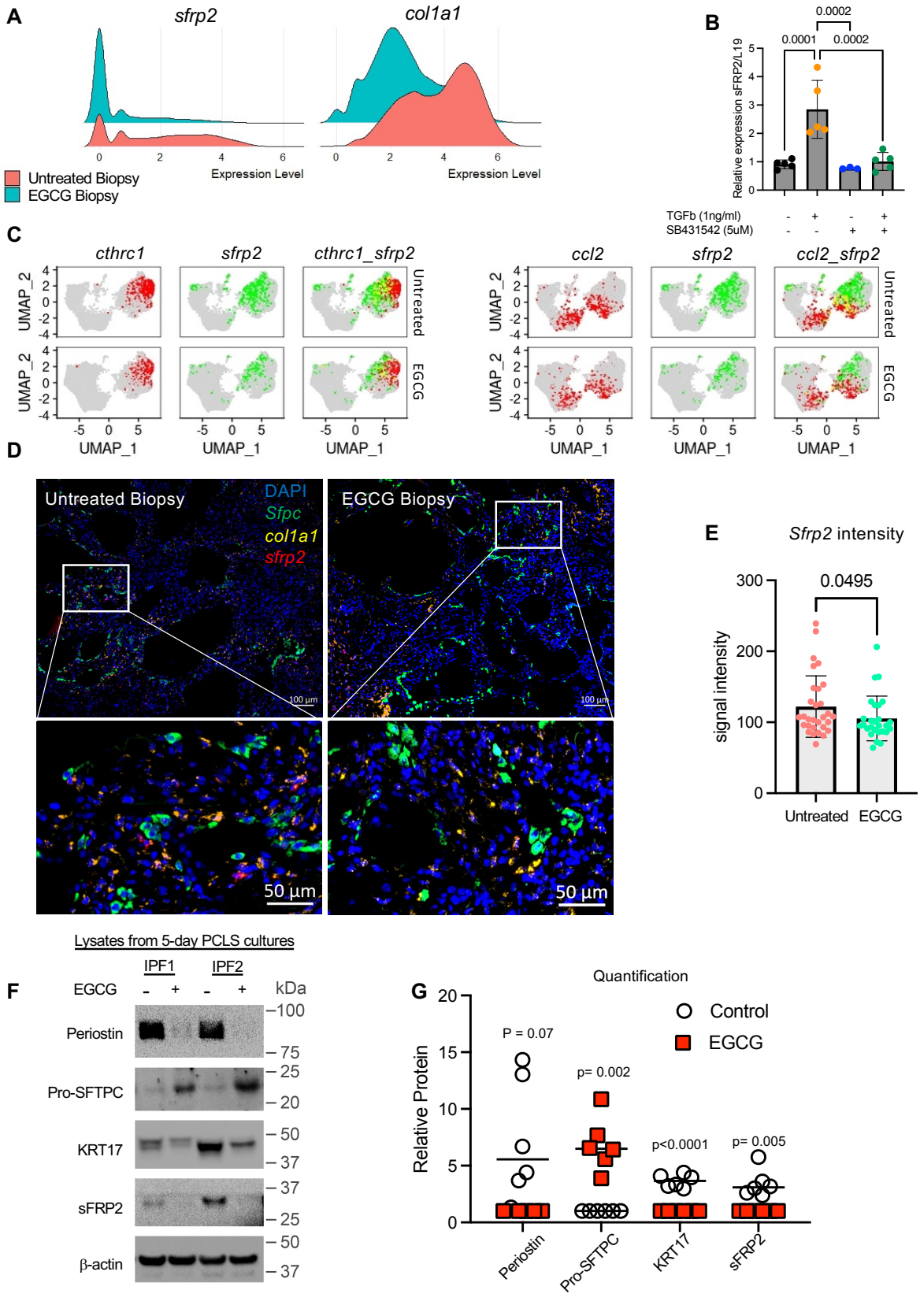
A
sfrp2
col1a1
Expression Level
Untreated Biopsy
EGCG Biopsy
B
Relative expression sFRP2/L19
0.0002
0.0001
0.0002
TGFb (1ng/ml)
SB431542 (5uM)
C
cthrc1
sfrp2
cthrc1_sfrp2
ccl2
ccl2_sfrp2
UMAP_1
UMAP_2
Untreated
EGCG
D
Untreated Biopsy
EGCG Biopsy
DAPI
Sfpc
col1a1
sfrp2
100 µm
50 µm
E
Sfrp2 intensity
0.0495
signal intensity
Untreated
EGCG
F
Lysates from 5-day PCLS cultures
IPF1
IPF2
EGCG
kDa
Periostin
Pro-SFTPC
KRT17
sFRP2
β-actin
G
Quantification
Control
EGCG
Relative Protein
P = 0.07
p= 0.002
p<0.0001
p= 0.005
Periostin
Pro-SFTPC
KRT17
sFRP2

Figure 4: : Impact of EGCG on distribution of sFRP2 expression in fibroblast subpopulations, biopsy tissues, and PCLS cultures.

(A) Ridge plot of *sfrp2* and *col1a1* gene expression in alveolar and pathologic fibroblasts subtypes from untreated and EGCG biopsy samples. **(B)** Relative expression of *sfrp2* mRNA in human fibroblasts treated with TGFβ1 (1 $ng.ml^{-1}$) and/or a TGFβ inhibitor SB4331542 (5μM) for 48 h (n=5)**. (C)** Feature plots of *sfrp2* gene expression (green) in various fibroblast subsets characterized by *cthrc1* or *ccl2* gene expression (red). Cells expressing both *sfrp2* and *cthrc1* or *ccl2* are indicated in yellow. Additional fibroblasts markers are shown in Supplemental Figure 4B. **(D, E)** RNA *in situ* hybridization was performed for *col1a1* (yellow) and *sfrp2* (red) gene in untreated and EGCG biopsies (**D**). The signal intensity of *sfrp2* was quantified in each image (**E**). Representative image of n=5 samples per group, 4-6 images per samples. Magnification x100 for top images. Bottom images represent an region of interest as indicated by white rectangle. **(F, G)** Precision-cut lung slices from IPF lung donors cultured for 7 days with EGCG (1μM) were analyzed by Western Blot. Additional samples are shown in Supplemental Figure 5C. (G) Graphical representation of the level of expression of selected proteins for all samples (Supplemental Figure 5C. n=6. Statistical significance was determined by the Kruskal–Wallis test (B) and 2-tailed t-test (E, G).

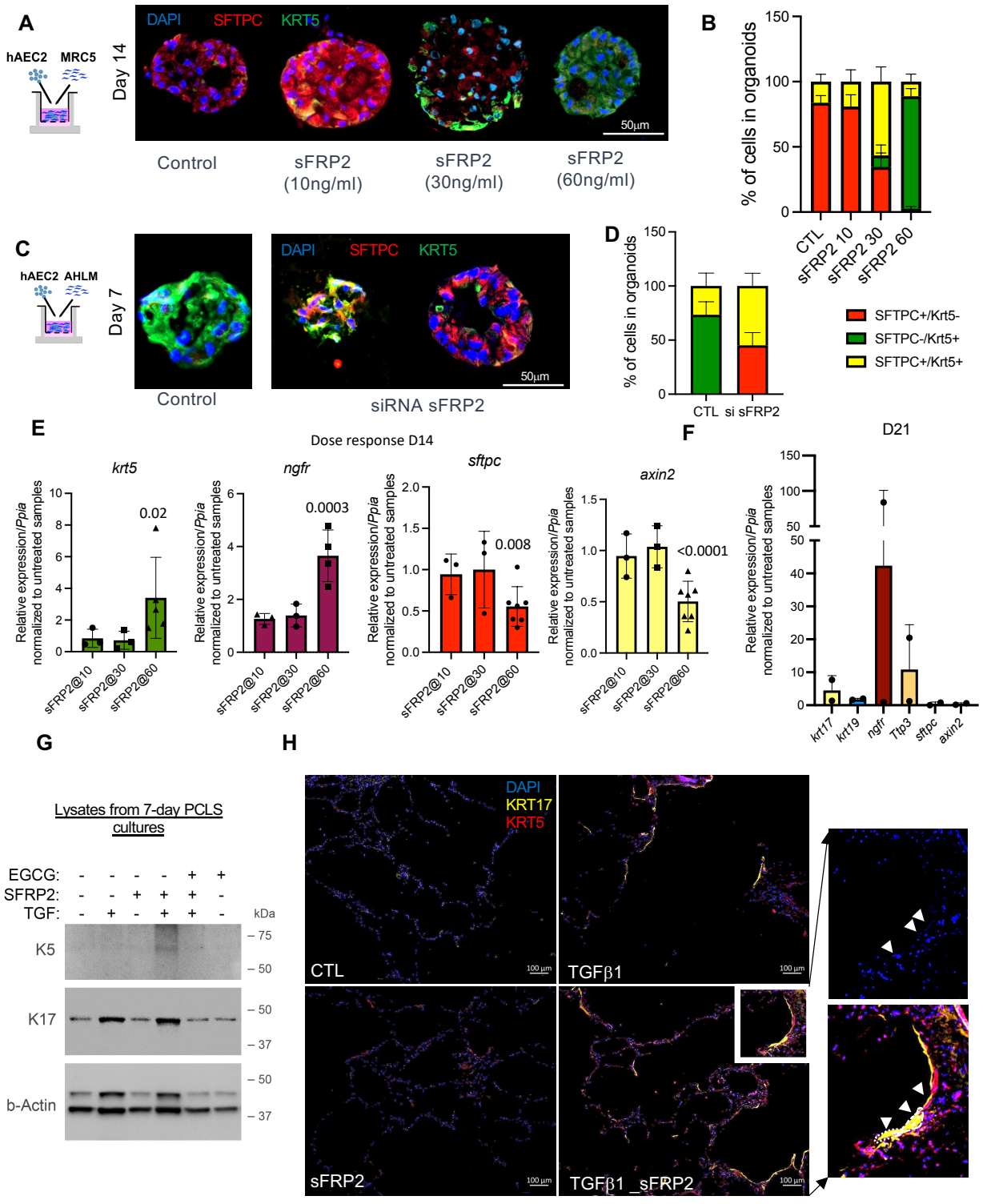
A
hAEC2
MRC5
Day 14
DAPI
SFTPC
KRT5
50µm
Control
sFRP2 (10ng/ml)
sFRP2 (30ng/ml)
sFRP2 (60ng/ml)
B
% of cells in organoids
CTL
sFRP2 10
sFRP2 30
sFRP2 60
C
hAEC2 AHLM
Day 7
Control
siRNA sFRP2
D
% of cells in organoids
CTL si sFRP2
SFTPC+/Krt5-
SFTPC-/Krt5+
SFTPC+/Krt5+
E
Dose response D14
krt5
ngfr
sftpc
axin2
Relative expression/Ppia normalized to untreated samples
0.02
0.0003
0.008
<0.0001
sFRP2@10
sFRP2@30
sFRP2@60
F
D21
krt17
krt19
ngfr
Ttp3
sftpc
axin2
G
Lysates from 7-day PCLS cultures
EGCG:
SFRP2:
TGF:
kDa
K5
K17
b-Actin
H
DAPI
KRT17
KRT5
CTL
TGFβ1
sFRP2
TGFβ1 _sFRP2

Figure 5

Figure 5: sFRP2 promotes basal cell differentiation of human AEC2s.

(A) Immunofluorescence for SFTPC and KRT5 of AEC2-derived organoids co-cultured with MRC5 cells treated sFRP2 for 14 days. Representative of n = 5 biologically replicates. The experiment was performed in three technical triplicates and data from three technical replicates are counted as one biological replicate. Magnification x200. (**B**) Percent of $SFTPC^{+}/KRT5^{-}$, $SFTPC^{+}/KRT5^{+}$, and $SFTPC^{-}/KRT5^{+}$ cells in day-14 AEC2s + MRC5 organoids treated with sFRP2. (**C**) Immunofluorescence of AEC2-derived organoids co-cultured with AHLM after sFRP2 silencing. Magnification x200. **(D)** Percent of $SFTPC^{+}/KRT5^{-}$, $SFTPC^{+}/KRT5^{+}$, and $SFTPC^{-}/KRT5^{+}$ cells in day-7 AEC2s + $AHLM^{sfrp2neg}$ organoids. Data are presented as the mean of n = 4 biological replicates. **(E)** Level of expression of *krt5*, *ngfr*, *sftpc*, and *axin2* mRNA in $EPCAM^{+}$ cells isolated from day-14 AEC2s + MRC5 organoids treated with sFRP2. n= 3 biological replicates for sFFRP2 (10 and 30ng.ml^{-1}) and n=4-7 biological replicates for sFRP2 (60 ng.ml^{-1}). **(F)** Expression of genes characteristic for basal cells in $EPCAM^{+}$ cells isolated from day-21 AEC2s + MRC5 organoids treated with sFRP2 (60 ng.ml^{-1}). n= 2 biological replicates. (**G-H**) Precision-cut lung slices from non-diseased donors were cultured and treated +/- TGFβ1 (2 ng.ml^{-1}) +/- sFRP2 (60 ng.ml^{-1}) +/- EGCG (1μM) for 7 days. (**G**) Lysates were blotted for KRT5 and KRT17. n= 3 biological replicates. (**H**) Immunofluorescence of KRT5 and KRT17. Representative of n = 3 independent experiments. Magnification x100. Region of interest is presented as an insert (white rectangle) to show elongation of nuclei (DAPI) and cell morphology, outlined as a doted line in insert as indicated by white arrows. Statistical significance was determined by mixed effects analysis followed by Tukey's multiple comparisons test (B, D), Dunnett's multiple comparisons test (E), and 2-tailed t-test (F). p-values are reported in Supplemental Table 4 for B and D.

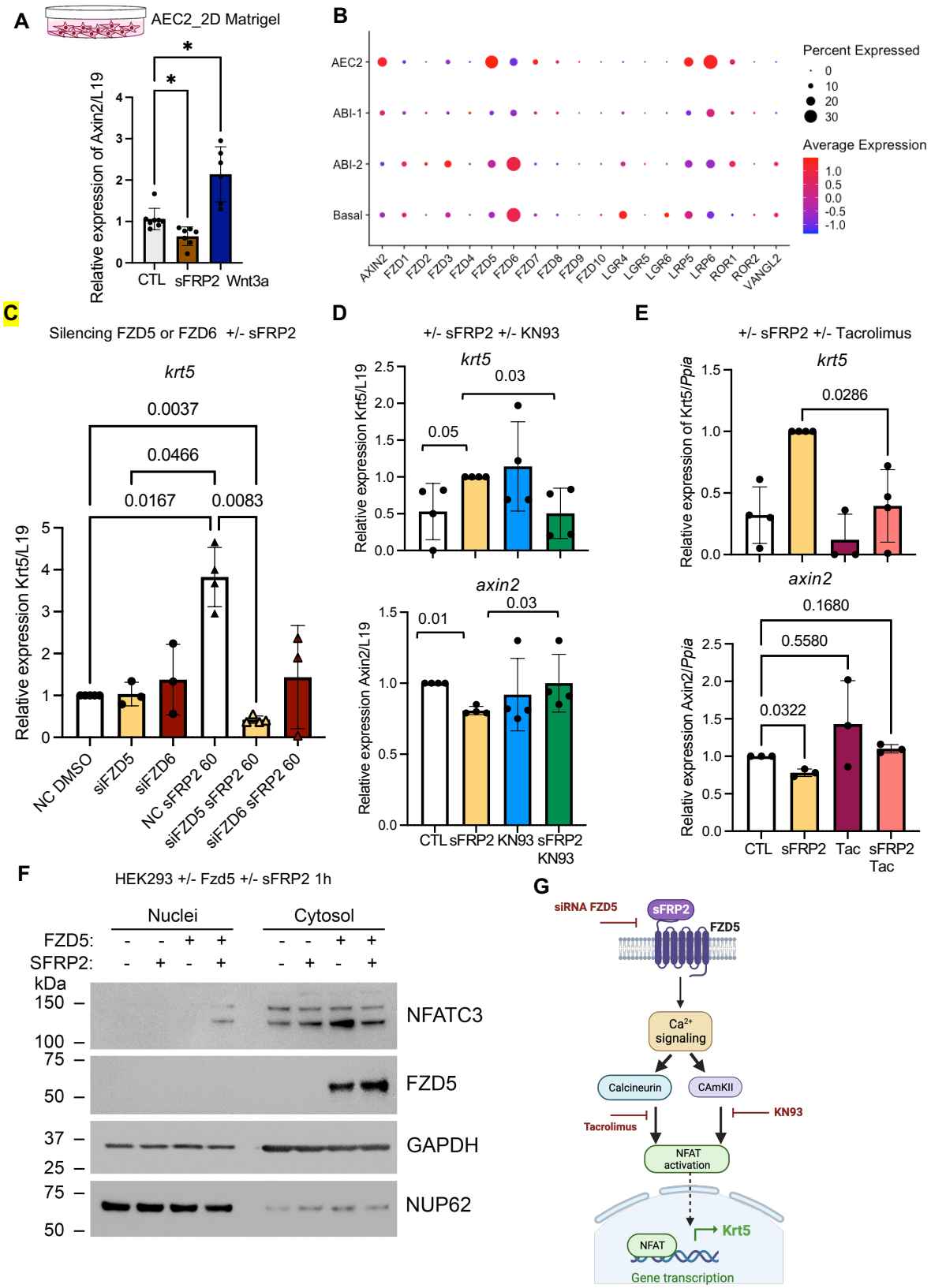
A
AEC2_2D Matrigel
Relative expression of Axin2/L19
CTL
sFRP2
Wnt3a
B
AEC2
ABI-1
ABI-2
Basal
AXIN2
FZD1
FZD2
FZD3
FZD4
FZD5
FZD6
FZD7
FZD8
FZD9
FZD10
LGR4
LGR5
LGR6
LRP5
LRP6
ROR1
ROR2
VANGL2
Percent Expressed
Average Expression
C
Silencing FZD5 or FZD6 +/- sFRP2
krt5
Relative expression Krt5/L19
NC DMSO
siFZD5
siFZD6
NC sFRP2 60
siFZD5 sFRP2 60
siFZD6 sFRP2 60
D
+/- sFRP2 +/- KN93
krt5
Relative expression Krt5/L19
axin2
Relative expression Axin2/L19
CTL
sFRP2
KN93
sFRP2 KN93
E
+/- sFRP2 +/- Tacrolimus
krt5
Relative expression of Krt5/Ppia
axin2
Relativ expression Axin2/Ppia
CTL
sFRP2
Tac
sFRP2 Tac
F
HEK293 +/- Fzd5 +/- sFRP2 1h
Nuclei
Cytosol
FZD5:
SFRP2:
kDa
NFATC3
FZD5
GAPDH
NUP62
G
siRNA FZD5
sFRP2
FZD5
Ca2+ signaling
Calcineurin
CAmKII
Tacrolimus
KN93
NFAT activation
NFAT
Krt5
Gene transcription

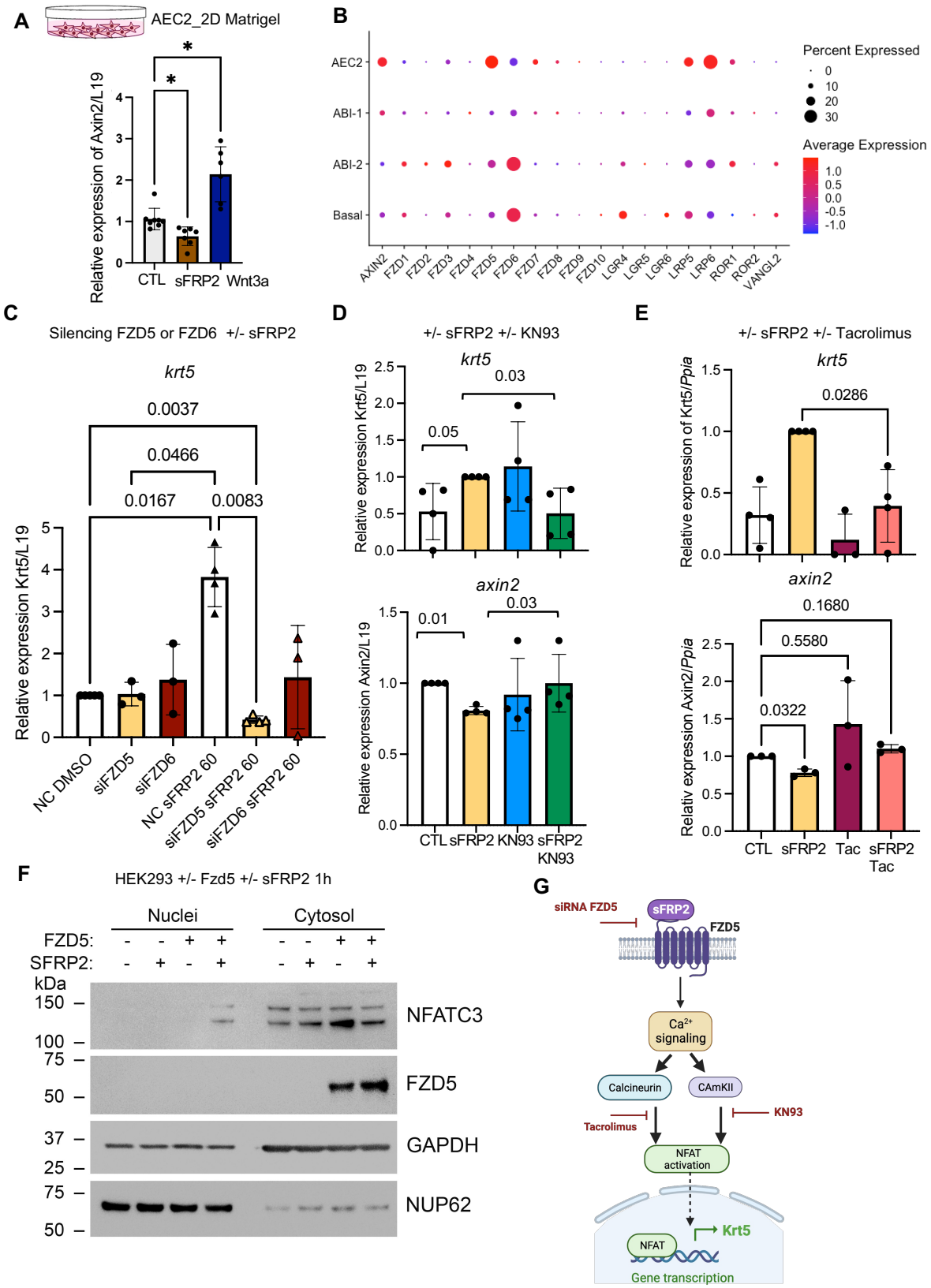
A
AEC2_2D Matrigel
Relative expression of Axin2/L19
CTL
sFRP2
Wnt3a
B
AEC2
ABI-1
ABI-2
Basal
AXIN2
FZD1
FZD2
FZD3
FZD4
FZD5
FZD6
FZD7
FZD8
FZD9
FZD10
LGR4
LGR5
LGR6
LRP5
LRP6
ROR1
ROR2
VANGL2
Percent Expressed
Average Expression
C
Silencing FZD5 or FZD6 +/- sFRP2
krt5
Relative expression Krt5/L19
NC DMSO
siFZD5
siFZD6
NC sFRP2 60
siFZD5 sFRP2 60
siFZD6 sFRP2 60
D
+/- sFRP2 +/- KN93
krt5
Relative expression Krt5/L19
axin2
Relative expression Axin2/L19
CTL
sFRP2
KN93
sFRP2 KN93
E
+/- sFRP2 +/- Tacrolimus
krt5
Relative expression of Krt5/Ppia
axin2
Relativ expression Axin2/Ppia
CTL
sFRP2
Tac
sFRP2 Tac
F
HEK293 +/- Fzd5 +/- sFRP2 1h
Nuclei
Cytosol
FZD5:
SFRP2:
kDa
NFATC3
FZD5
GAPDH
NUP62
G
siRNA FZD5
sFRP2
FZD5
Ca2+ signaling
Calcineurin
CAmKII
Tacrolimus
KN93
NFAT activation
NFAT
Krt5
Gene transcription

Figure 6: sFRP2 acts on AEC2s through the Fzd5 receptor to promote noncanonical Wnt signaling.

(A) *axin2* gene expression in AEC2s cultured for 48 h with sFRP2 (60 ng.ml^{-1}) or Wnt3a (100ng.ml^{-1}). N = 4-6 biological replicates. **(B)** DotPlot of Frizzled receptors and related coreceptors from selected epithelial cells from donor, control biopsy, and ILD explant samples. **(C)** *krt5* mRNA level expressed in AEC2s were measured after silencing the expression of *fzd5* or *fzd6*. The silenced *fzd5* and silenced *fzd6* AEC2 were subsequently treated with 60 ng.ml^{-1} of sFRP2 for 48 h. n= 3 independent biological replicates. (**D**) Level of expression of *krt5* and *axin2* mRNA were measured in AEC2 cells treated with CaMKII inhibitor KN93 (1ug.ml^{-1}) with or without sFRP2 (60ng.ml^{-1}) for 48 h. (**E**) Level of expression of *krt5* and *axin2* mRNA were measured in AEC2 cells treated with Tacrolimus (1μM) with or without sFRP2 (60ng.ml^{-1}) for 48 h. **(F)** Western blot indicating the presence of NFATC3 in nuclei extract from HEK-293 cells transfected with FZD5 plasmid followed by treatment with sFRP2 (30ng.ml^{-1}) for 1 h. n=3 biological replicates. **(G)** Schematic of the sFRP2-FZD5 signaling pathway promoting the expression of KRT5 in AECs created with BioRender.com. Statistical significance was determined by Kruskal-Wallis (A) or Tukey's (C) or Dunnett's (*axin2* in E) and Mann Whitney t-test (D, *krt5* in E).